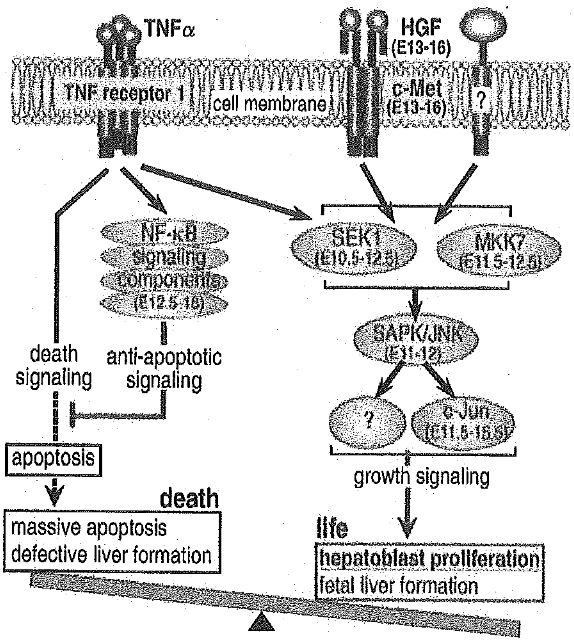

Fig. 1. **A proposed model for SAPK/JNK signaling pathway in hepatoblasts.** The numbers in parentheses are dates of embryonic lethality reported in previous papers. TNFα elicits a wide range of biological responses, such as inflammation, tumor necrosis, differentiation, cell proliferation, and apoptosis, through the stimulation of its receptor, TNFR1. The induction of apoptosis, NF-κB activation, and SAPK/JNK activation are simultaneously mediated through TNFR1. SAPK/JNK activation is involved in cell proliferation, while activation of NF-κB protects against the apoptosis in hepatoblasts (*13*).

caspase 3 activation, even though *apaf1*$^{-/-}$ ES cells exhibit profound defects in the mitochondria-dependent apoptosis (*17*). In those *sek1*$^{-/-}$ *mkk7*$^{-/-}$ ES cells, the SAPK/JNK activation by various stresses was completely abolished. Normal apoptotic responses without SAPK/JNK activation were also observed in fibroblasts derived from *sek1*$^{-/-}$ *mkk7*$^{-/-}$ ES cells. These results raised the question of whether SAPK/JNK activation is indeed required for the induction of cell death in response to apoptosis inducers. Thus, the physiological role of SAPK/JNK activation in cell survival and apoptosis is controversial, being suggested to have a pro-apoptotic, an anti-apoptotic, or no function (*18*).

From our recent results, it appears that the various roles of SAPK/JNK activation in apoptosis depend on the cell types and conditions observed. While late passage *mkk7*$^{-/-}$ MEFs are resistant to cell death in the same manner as *Jnk1*$^{-/-}$ *Jnk2*$^{-/-}$ and *sek1*$^{-/-}$ *mkk7*$^{-/-}$ MEFs (*15*, *16*), *mkk7*$^{-/-}$ MEFs at earlier cell passages (passages 1–4) undergo apoptosis in response to UV exposure with the same kinetics and to the same extent as wild-type MEFs (*14*). These results support the notion that SAPK/JNK activation is not always involved in apoptosis, but this activation rather regulates apoptosis in a signal-specific (and perhaps cell type-dependent) manner. Our results in MEFs indicate that the 'history' and passage number of

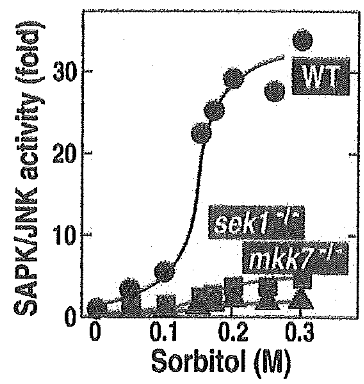

Fig. 2. **SAPK/JNK activation in response to hyper-osmolar stress (sorbitol) requires both SEK1 and MKK7 in ES cells.** Wild-type, *sek1*$^{-/-}$, and *mkk7*$^{-/-}$ ES cells were stimulated with the indicated concentrations of sorbitol for 30 min.

cells is a critical determinant of cell death susceptibility in the absence of MKK7 expression.

SAPK/JNK activation as a molecular switch in an all-or-none manner

Recently, Ferrell *et al.* have proposed the interesting concept that SAPK/JNK-signaling cascade could, in principle, function as a sensitivity amplifier, which converts graded inputs into more switch-like outputs, allowing the cascade to filter out noise and yet still respond decisively to supra-threshold stimuli (*19*, *20*). They have shown in *Xenopus* oocytes, HeLa cells, HEK293 cells, and Jurkat T cells that SAPK/JNK responds to physiological and pathological stimuli, such as progesterone and sorbitol, in an all-or-none manner. The activation of SAPK/JNK by the stimuli was graded at the level of a population of oocytes; however, at the level of an individual oocyte, the stimulatory response appeared to be switch-like. Indeed, we have also observed a very steep concentration-dependent response in the activation of SAPK/JNK by hyper-osmolar stress, sorbitol, in wild-type murine embryonic stem (ES) cells but not in *sek1*$^{-/-}$ and *mkk7*$^{-/-}$ cells (Fig. 2) (*21*). This suggests that the all-or-none type MAPK activation also occurs in mammalian cells at an individual cell level only when the two MAPKKs are simultaneously activated. Therefore, this MAPK signaling should strictly proceed without errors basically through two separate signals, one that activates SEK1 and one that activates MKK7. The full activation of SAPK/JNK by SEK1 and MKK7 may be required for hepatoblast proliferation (Fig. 1).

Molecular mechanism of SAPK/JNK activation in living cells

Activation of SAPK/JNK requires the dual phosphorylation of Tyr and Thr residues located in a Thr-Pro-Tyr motif in the activation loop between VII and VIII of the kinase domain. The phosphorylation is catalyzed by the dual specificity kinases, SEK1 and MKK7, which are capable of catalyzing the phosphorylation of both Thr and Tyr residues. Recent studies have shown that SEK1 preferentially phosphorylates the Tyr residue, and MKK7 the

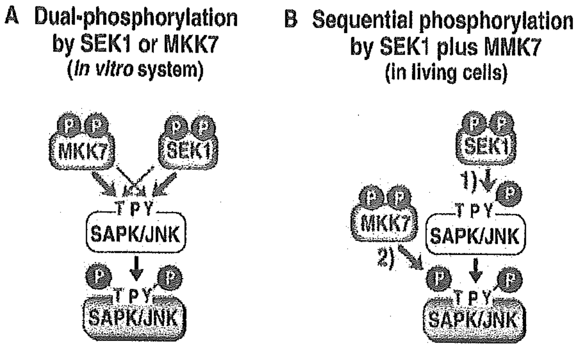

Fig. 3. **Schematic description of SAPK/JNK phosphorylation by SEK1 and MKK7 *in vitro* and *in vivo*.** A: Synergistic activation of SAPK/JNK by the dual-specificity kinase, SEK1 or MKK7, which has been reported in *in vitro* conditions (*22–24*). B: Synergistic activation of SAPK/JNK through sequential phosphorylation by SEK1 and MKK7 in murine living cells (*21, 25*). TPY, Thr-Pro-Tyr motif.

Thr residue of SAPK/JNK *in vitro* (Fig. 3A) (*22–24*). Strong support for this activation mechanism has been obtained from studies of SEK1- and MKK7-gene disruption in ES cells (*21, 25*). The severe impairment of SAPK/JNK activation observed in *mkk7*$^{-/-}$ ES cells was accompanied by a loss of the Thr-phosphorylation of SAPK/JNK, without marked reduction in its Tyr-phosphorylation level. On the other hand, Thr-phosphorylation of SAPK/JNK in *sek1*$^{-/-}$ ES cells was also attenuated, in addition to a decreased level of its Tyr-phosphorylation. These results indicate that the Tyr and Thr residues of SAPK/JNK are sequentially phosphorylated by SEK1 and MKK7, respectively, in stress-stimulated living cells (Fig. 3B).

Conclusion

SAPK/JNK activation by SEK1 and MKK7 is required for embryonic hepatoblast proliferation. The full activation of SAPK/JNK occurs only when the two MAPKKs are simultaneously activated. The Tyr and Thr residues of SAPK/JNK are sequentially phosphorylated by SEK1 and MKK7, respectively, in living cells.

SAPK/JNK may either protect or enhance sensitivity to apoptosis depending on the cell type, stimuli, and the latency of the activation of the MAPK. Our recent results in MEFs indicate that the "history" and passage number of cells are a critical determinant of cell death susceptibility in the absence of MKK7 expression. In this apoptotic pathway, SAPK/JNK seems to function through its effects on gene expression but not a direct effect on the effectors of apoptosis. These new findings could also solve the controversial data that have been obtained in different cell types and in different laboratories.

REFERENCES

1. Davis, R.J. (2000) Signal transduction by the JNK group of MAP kinases. *Cell* **103**, 239–252
2. Chang, L. and Karin, M. (2001) Mammalian MAP kinase signalling cascades. *Nature* **410**, 37–40
3. Weston, C.R. and Davis, R.J. (2002) The JNK signal transduction pathway. *Curr. Opini. Genes Dev.* **12**, 14–21
4. Manning, A.M. and Davis, R.J. (2003) Targeting JNK for therapeutic benefit: from junk to gold? *Nat. Rev. Mol. Drug Disc.* **2**, 554–565
5. Nishina, H., Nakagawa, K., Azuma, N., and Katada, T. (2003) Activation mechanism and physiological roles of stress-activated protein kinase/c-Jun NH_2-terminal kinase in mammalian cells. *J. Biol. Regul. Homeost. Agents.* **17**, 295–302
6. Wada, T. and Penninger, J.M. (2004) Mitogen-activated protein kinases in apoptosis regulation. *Oncogene* **23**, 2838–2849
7. Kuan, C.Y., Yang, D.D., Roy, D.R., Davis, R.J., Rakic, P., and Flavell, R.A. (1999) The Jnk1 and Jnk2 protein kinases are required for regional specific apoptosis during early brain development. *Neuron* **22**, 667–676
8. Sabapathy, K., Jochum, W., Hochedlinger, K., Chang, L., Karin, M., and Wagner, E.F. (1999) Defective neural tube morphogenesis and altered apoptosis in the absence of both JNK1 and JNK2. *Mech. Dev.* **89**, 115–124
9. Nishina, H., Fischer, K.D., Radvanyi, L., Shahinian, A., Hakem, R., Rubie, E.A., Bernstein, A., Mak, T.W., Woodgett, J.R., and Penninger, J.M. (1997) Stress-signalling kinase Sek1 protects thymocytes from apoptosis mediated by CD95 and CD3. *Nature* **385**, 350–353
10. Yang, D., Tournier, C., Wysk, M., Lu, H.T., Xu, J., Davis, R.J., and Flavell, R.A. (1997) Targeted disruption of the MKK4 gene causes embryonic death, inhibition of c-Jun NH2-terminal kinase activation, and defects in AP-1 transcriptional activity. *Proc. Natl Acad. Sci. USA* **94**, 3004–3009
11. Ganiatsas, S., Kwee, L., Fujiwara, Y., Perkins, A., Ikeda, T., Labow, M.A., and Zon, L.I. (1998) SEK1 deficiency reveals mitogen-activated protein kinase cascade crossregulation and leads to abnormal hepatogenesis. *Proc. Natl Acad. Sci. USA* **95**, 6881–6886.
12. Nishina, H., Vaz, C., Billia, P., Nghiem, M., Sasaki, T., Pompa, J.L., Furlonger, K., Paige, C., Hui, C.-C., Fischer, K.D., Kishimoto, H., Iwatsubo, T., Katada, T., Woodgett, J.R., and Penninger, J.M. (1999) Defective liver formation and liver cell apoptosis in mice lacking the stress signaling kinase SEK1/MKK4. *Development* **126**, 505–516
13. Watanabe, T. Nakagawa, K, Ohata, S, Kitagawa, D., Nishitai, G., Seo, J., Tanemura, S., Shimizu, N., Kishimoto, H., Wada, T., Aoki, J., Arai, H., Iwatsubo, T., Mochita, M., Watanabe, T., Satake, M., Ito, Y., Matsuyama, T., Mak, T.W., Penninger, J.M., Nishina, H., and Katada, T. (2002) SEK1/MKK4-mediated SAPK/JNK signaling participates in embryonic hepatoblast proliferation via a pathway different from NF-κB-induced anti-apoptosis. *Dev. Biol.* **250**, 332–347
14. Wada, T., Joza, N., Cheng, H.-Y.M., Sasaki, T., Kozieradzki, I., Bachmaier, K., Katada, T., Schreiber, M., Wagner, E.F., Nishina, H., and Penninger, J.M. (2004) MKK7 couples stress signaling to G2/M cell cycle progression and cellular senescence. *Nat. Cell Biol.* **6**, 215–226
15. Tournier, C., Hess, P., Yang, D.D., Xu, J., Turner, T.K., Nimnual, A., Bar-Sagi, D., Jones, S.N., Flavell, R.A., and Davis, R.J. (2000) Requirement of JNK for stress-induced activation of the cytochrome c–mediated death pathway. *Science* **288**, 870–874
16. Tournier, C., Dong, C., Turner, T.K., Jones, S.N., Flavell, R.A., and Davis, R.J. (2001) MKK7 is an essential component of the JNK signal transduction pathway activated by proinflammatory cytokines. *Genes Dev.* **15**, 1419–1426
17. Nishitai, G., Shimizu, N., Negishi, T., Kishimoto, H., Nakagawa, K., Kitagawa, D., Watanabe, T., Momose, H., Ohata, S., Tanemura, S., Asaka, S., Kubota, J., Saito, R., Yoshida, H., Mak, T.W., Wada, T., Penninger, J.M., Azuma, N., Nishina, H., and Katada, T. (2003) Stress induces mitochondria-mediated apoptosis independent of SAPK/JNK activation in ES cells. *J. Biol. Chem.* **279**, 1621–1626
18. Lin, A. (2002) Activation of the JNK signaling pathway: breaking the brake on apoptosis. *Bioessays* **25**, 17–24

19. Bagowski, C.P. and Ferrell, J.E. (2001) Bistability in the JNK cascade. *Curr. Biol.* **11**, 1176–1182
20. Bagowski, C.P., Besser, J., Frey, C.R., Ferrell, J.E. (2003) The JNK cascade as a biochemical switch in mammalian cells: Ultrasensitive and all-or-none responses. *Curr. Biol.* **13**, 315–320
21. Kishimoto, H., Nakagawa, K., Watanabe, T., Kitagawa, D., Momose, H., Seo, J., Nishitai, G., Shimizu, N., Ohata, S., Tanemura, S., Asaka, S., Goto, T., Fukushi, H., Yoshida, H., Suzuki, A., Sasaki, T., Wada, T., Penninger, J.M., Nishina, H., and Katada, T. (2003) Different Properties of SEK1 and MKK7 in Dual Phosphorylation of Stress-induced Activated Protein Kinase SAPK/JNK in Embryonic *Stem Cells. J. Biol. Chem.* **278**, 16595–16601
22. Lawler, S., Fleming, Y., Goedert, M., and Cohen, P. (1998) Synergistic activation of SAPK1/JNK1 by two MAP kinase kinases *in vitro*. *Curr. Biol.* **8**, 1387–1390
23. Lisnock, J., Griffin, P., Calaycay, J., Franz, B., Parsons, J., O'Keefe, S.J., and LoGrasso, P. (2000) Activation of JNK3α1 requires both MKK4 and MKK7: Kinetic characterization of *in vitro* phosphorylated JNK3α1. *Biochemistry* **39**, 3141–3148
24. Fleming, Y., Armstrong, C.G., Morrice, N., Paterson, A., Goedert, M., and Cohen, P. (2000) Synergistic activation of stress-activated protein kinase 1/c-Jun N-terminal kinase (SAPK1/JNK) isoforms by mitogen-activated protein kinase 4 (MKK4) and MKK7. *Biochem. J.* **352**, 145–154
25. Wada, T., Nakagawa, K., Watanabe, T., Nishitai, G., Seo, J., Kishimoto, H., Kitagawa, D., Sasaki, T., Penninger, J.M., Nishina, H., and Katada, T. (2001). Impaired synergistic activation of stress activated protein kinase SAPK/JNK in mouse embryonic stem cells lacking SEK1/MKK4. *J. Biol. Chem.* **276**, 30892–30897

Journal of Neuroscience Research 76:265–276 (2004)

Blockade of Interleukin-6 Receptor Suppresses Reactive Astrogliosis and Ameliorates Functional Recovery in Experimental Spinal Cord Injury

S. Okada,[1–3] M. Nakamura,[4] Y. Mikami,[4] T. Shimazaki,[1,3] M. Mihara,[5] Y. Ohsugi,[5] Y. Iwamoto,[2] K. Yoshizaki,[6] T. Kishimoto,[7] Y. Toyama,[4] and H. Okano[1,3]*
[1]Department of Physiology, Keio University School of Medicine, Shinjuku, Tokyo, Japan
[2]Department of Orthopedic Surgery, Graduate School of Medical Sciences, Kyushu University, Fukuoka, Japan
[3]Core Research for Evolutional Science and Technolory (CREST), Japan Science and Technology Agency (JST), Kawaguchi, Saitama, Japan
[4]Department of Orthopedic Surgery, Keio University School of Medicine, Shinjuku, Tokyo, Japan
[5]Chugai Pharmaceutical Company Ltd., Tokyo, Japan
[6]Department of Medical Science I, School of Health and Sport Sciences, Osaka University, Suita, Osaka, Japan
[7]Department of Immunology, Graduate School of Frontier Biosciences Osaka University, Suita, Osaka, Japan

Endogenous neural stem/progenitor cells (NSPCs) have recently been shown to differentiate exclusively into astrocytes, the cells that are involved in glial scar formation after spinal cord injury (SCI). The microenvironment of the spinal cord, especially the inflammatory cytokines that dramatically increase in the acute phase at the injury site, is considered to be an important cause of inhibitory mechanism of neuronal differentiation following SCI. Interleukin-6 (IL-6), which has been demonstrated to induce NSPCs to undergo astrocytic differentiation selectively through the JAK/STAT pathway in vitro, has also been demonstrated to play a critical role as a proinflammatory cytokine and to be associated with secondary tissue damage in SCI. In this study, we assessed the efficacy of rat anti-mouse IL-6 receptor monoclonal antibody (MR16-1) in the treatment of acute SCI in mice. Immediately after contusive SCI with a modified NYU impactor, mice were intraperitoneally injected with a single dose of MR16-1 (100 μg/g body weight), the lesions were assessed histologically, and the functional recovery was evaluated. MR16-1 not only suppressed the astrocytic diffentiation-promoting effect of IL-6 signaling in vitro but inhibited the development of astrogliosis after SCI in vivo. MR16-1 also decreased the number of invading inflammatory cells and the severity of connective tissue scar formation. In addition, we observed significant functional recovery in the mice treated with MR16-1 compared with control mice. These findings suggest that neutralization of IL-6 signaling in the acute phase of SCI represents an attractive option for the treatment of SCI. © 2004 Wiley-Liss, Inc.

Key words: spinal cord injury; IL-6; glial scar; inflammation; neural stem/progenitor cells

Recent studies have shown the existence of neural stem/progenitor cells (NSPCs) in adult mammalian spinal cord and have raised the possibility that the spinal cord has latent capacity for self-repair in response to injury or disease through the use of endogenous NSPCs (Horner et al., 2000; Bjorklund and Lindvall, 2000). After a spinal cord injury (SCI), however, these cells proliferate and migrate to the lesion site, where they differentiate exclusively into astrocytes, never into neurons, and are eventually associated with glial scar formation (Johansson et al., 1999; Takahashi et al., 2003). Glial scar tissue is considered a physical barrier and prevents axonal regeneration by producing axonal growth inhibitors, such as chondroitin sulfate proteoglycans (David and Lacroix, 2003). The major causes of this inhibitory mechanism of neuronal differentiation include the microenvironmental factors that dramatically change immediately following SCI. The interleukin (IL)-6 family of cytokines has been shown to play especially important roles in regulating the various biological responses through multichain receptor complexes-mediated signaling (for review see Taga and Kishimoto, 1997). The multichain receptor complexes, which include the ligand binging receptor (e.g., IL-6-

Contract grant sponsor: Japanese Ministry of Education, Sports and Culture; Contract grant sponsor: Human Frontier Science Program Organization; Contract grant sponsor: Core Research for Evolutional Science and Technology (CREST).

*Correspondence to: Hideyuki Okano, Department of Physiology Keio University School of Medicine, 35 Shinanomachi, Shinjuku, Tokyo, 160-8582, Japan. E-mail: hidokano@sc.itc.keio.ac.jp

Received 8 July 2003; Revised 14 October; Accepted 5 November

Published online 8 March 2004 in Wiley InterScience (www.interscience.wiley.com). DOI: 10.1002/jnr.20044

receptor) and nonligand binding membrane glycoprotein gp130 (Taga et al., 1989), have been shown to play essential roles in signal transduction of the IL-6 family of cytokines. Many lines of evidences suggest that this family of cytokines plays important roles in regulating the immune response (Taga and Kishimoto, 1997), inflammation, and central nervous system (CNS) development and significantly increases in the spinal cord after it is injured (Pan et al., 2002; Nakamura et al., 2003), and gp130-mediated signaling has been demonstrated to induce astrocytic differentiation of NSPCs through the JAK/STAT pathway in vitro (Bonni et al., 1997; Nakashima et al., 1999), suggesting the possibility that blockade of IL-6 trans-signaling after SCI may diminish the reactive astrogliosis and ameliorate functional recovery. Moreover, the IL-6 released during the acute phase of SCI promotes the inflammatory cell chemotaxis and is involved in the secondary injury cascade that is mediated by active inflammatory cell and molecular processes. A recent study has shown that excess activation of gp130 signaling by hyper-IL-6 (a bioactive IL-6/sIL-6R fusion protein) following SCI is associated with a robust inflammatory and glial response that appears to reduce axonal outgrowth in the adult mammalian CNS (Lacroix et al., 2003).

In this study, we used a murine SCI model to investigate the effects of blockade of IL-6 signaling with a monoclonal antibody against the IL-6 receptor (MR16-1, a rat monoclonal antibody that is known to bind to the mouse IL-6-receptor and block the Il-6-mediated cellular responses; Tamura et al., 1993; Takagi et al., 1998; Katsume et al., 2002; Okazaki et al., 2002). We examined whether MR16-1 treatment would offer the promise of a new therapeutic strategy for treating SCI. The results showed that MR16-1 suppressed not only the glial differentiation of NSPCs caused by IL-6 signaling in vitro but also the astrogliosis after SCI in vivo. MR16-1 also decreased infiltration by inflammatory cells and scar tissue formation at the lesion site. In addition, the MR16-1-treated mice showed significantly better functional recovery than the nontreated mice.

MATERIALS AND METHODS

Animals

In total, 74 adult female C57BL/6J mice (18–22 g, 8–10 weeks of age) were used for this study. The ethics committee of our institution approved all surgical interventions and animal care procedures, which were in accordance with the Laboratory Animal Welfare Act, the *Guide for the Care and Use of Laboratory Animals* (National Institutes of Health), and the Guidelines and Policies for Animal Surgery provided by the Animal Study Comittees of the Central Institute for Experimental Animals and of Keio University.

Rat Anti-Mouse IL-6 Receptor Monoclonal Antibody (MR16-1)

The rat anti-mouse IL-6 receptor monoclonal antibody, MR16-1, was prepared as described previously (Tamura et al., 1993). The isotype of this antibody was Ig-G1. MR16-1 was shown to bind to the soluble IL-6 receptor of the mouse and suppress IL-6-induced cellular responses in a dose-dependent fashion (Okazaki et al., 2002). Other basic characterizations of this antibody have been described in previously published reports (Tamura et al., 1993; Okazaki et al., 2002).

Primary Cultures and Passaging Procedures

Spinal cord tissue was dissected from adult mice and transferred into Hank's balanced salt solution (HBSS) containing trypsin (1.33 mg/ml), hyaluronidase (0.67 mg/ml), and kynurenic acid (0.2 mg/ml; all from Sigma, St. Louis, MO) and then minced. After digestion for 4 min at 37°C, the tissue was transferred to HBSS containing trypsin inhibitor (0.7 mg/ml; Roche Diagnostics, Mannheim, Germany) and DNase (0.01 mg/ml; Boehringer Mannheim, Indianapolis, IN). Cells and tissue fragments were washed once with DMEM containing 10% fetal bovine serum (FBS; Hyclone, Logan, UT) and dissociated with a 5-ml pipette. Whole digested tissue was washed again and suspended in DMEM-10% FBS, filtered through sterile 100-mm nylon mesh, and thoroughly mixed with an equal volume of Percoll solution. The cell suspension was fractionated by centrifugation for 30 min, 18°C at 12,300 rpm. Cell fractions were harvested and washed free of Percoll by three rinses in DMEM/10% FBS. After a final centrifugation, the cell suspension was harvested in standard neurosphere culture medium and propagated as described previously (Reynolds and Weiss, 1992; Shimazaki et al., 2001). After the neurosphere-like cell masses had grown to near-confluence, they were passaged and replated at a density of 2×10^5 cells/ml. For differentiation assay, spheres passaged five or six times were dissociated into single cells and plated onto poly-L-ornithine (PO)-coated coverslips at a density of 5×10^5 cells/ml. To investigate the effects of IL-6 signaling on the neural progenitors, we added both IL-6 and soluble IL-6 receptor to the culture medium. As reviewed by Van Wagoner and Benveniste (1999), unlike most soluble receptors that act as antagonists to their respective ligands, the soluble receptor of IL-6 has been shown to function as an agonist of the IL-6-mediated cellular responses by binding to the nonligand binding glycoprotein gp130 (Taga et al., 1989), which acts as a signal transducer of the IL-6 family of cytokines (Taga and Kishimoto, 1997). In the present study, the dissociated adult mouse spinal cord-derived neural precursor cells that had been prepared as described above, were allowed to differentiate for 3 days in the presence of IL-6 (20 ng/ml) and soluble IL-6 receptor-α (sIL-6R; 20 ng/ml), with or w/o MR16-1 (25 μg/ml).

Spinal Cord Injury Model

Female C57BL/6J mice were anesthetized with an intraperitoneal injection of ketamine (100 mg/kg) and xylazine (10 mg/kg). After laminectomy at the T9 level, the dorsal surface of dura matter was exposed. The vertebral column was stabilized with fine forceps and clamps at the T7 and T10 spinous processes and ligament, and the animal's body was then lifted. SCI was induced with a modified NYU impactor (Gruner, 1992; Kuhn and Wrathall, 1998; Jakeman et al., 2000). A 3-g weight (1.2-mm-diameter tip) was allowed to drop from a height of 25 mm onto the dorsal surface of the dura matter. The muscles and the incision were then closed in layers, and the animals were placed in a temperature-controlled chamber until thermoregulation was reestablished. Manual bladder expression was performed twice per day until reflex bladder emptying was reestablished.

Injection of MR16-1 and BrdU

Immediately after the SCI, mice were intraperitoneally injected with a single dose of MR 16-1 (100 μg/g body weight; MR16-1 group) or with the same volume and concentration of purified rat IgG (ICN/Cappel Ohio; control group). To label the cells that divided after the injury, a sterile solution of bromodeoxyuridine (BrdU; 50 μg/g body weight; Sigma) was intraperitoneally injected daily for 2 weeks after the SCI.

Behavioral Analysis

Three different tests were used to assess recovery of motor function after SCI. We examined 30 injured mice (15 animals per group) for functional evaluation. Each mouse was tested at 1, 3, 5, and 7 days postoperatively and weekly thereafter until 6 weeks. Every test was performed in a double-blind fashion and recorded on videotape.

Open-field locomotion. Motor function of the hindlimbs was evaluated by the locomotor rating test on the Basso-Beattie-Bresnahan (BBB) scale, as described previously (Basso et al., 1996). A team of three experienced examiners evaluated each animal for 4 min and assigned an operationally defined score for each hindlimb.

SCANET. Motor function was evaluated with a SCANET automated motion-analysis system (MV-10, Toyo Sangyo Co., Ltd., Toyama, Japan) developed to measure spontaneous motor activity in small animals. SCANET consists of a cage equipped with two crossing sensor frames arranged at different heights that allow monitoring of small (M1) and large (M2) horizontal movements plus the vertical movement involved in rearing (RG). The M1 and M2 scores represent total distances moved, and the RG score represents the frequency of vertical movements within a certain period, which is useful for assessing recovery of limb function after SCI in mice, as reported previously (Mikami et al., 2002). Each mouse was individually placed in the SCANET cage, and its spontaneous locomotor activity was measured for 10 min.

Rota-rod treadmill. Motor coordination was assessed with a rotating rod apparatus (Muromachi Kikai Co., Ltd., Tokyo, Japan), consisting of a plastic rod (3 cm diameter, 8 cm long) with a gritted surface, flanked by two large discs (40 cm diameter). A mouse was placed on the rod, and the rod was rotated at speeds of 5, 10, and 15 rpm. Latency until a fall occurred was monitored for 120 sec (Ogura et al., 2001). Three trials were conducted at each speed, and the average and maximum numbers of seconds were recorded.

Immunohistochemistry

At 2 weeks after the SCI, animals in both the MR16-1 group and the control group were deeply anesthetized by inhalation of diethyl ether and transcardially perfused with 4% paraformaldehyde in 0.1 M phosphate-buffered saline (PBS) for histological studies. Spinal cord tissue was removed and post-fixed with 4% paraformaldehyde in PBS for a few hours at room temperature. Tissue samples were immersed in 10% sucrose in PBS at 4°C for 24 hr, placed in 30% sucrose in PBS for 48 hr, and embedded in OTC compound. The embedded tissue was immediately frozen in liquid nitrogen and stored at −80°C until needed. Frozen sections of spinal cord 20 μm thick were cut on a cryostat in the axial and sagittal plane and stained with hematoxylin and eosin. For the immunofluorescence double-labeling experiment, spinal cord sections were permeabilized with 0.03% Triton X-100 and 10% normal goat serum in 0.01 M PBS, pH 7.4, for 30 min. As primary antibodies, rat anti-BrdU 1:200 (Abcam, Cambridge, United Kingdom), rabbit anti-GFAP antibody 1:1000 (Dako, Carpinteria, CA), rat anti-Mac-1 1:200 (Pharmingen, San Diego, CA), or human anti-Hu 1:2,000 (a gift from Dr. Robert Darnell, The Rockefeller University) were applied to the sections at 4°C overnight. The sections were then incubated with secondary antibodies conjugated with Texas red, fluorescein isothiocyanate (FITC; all from Jackson Immunoresearch, West Grove, PA) for 1 hr at room temperature. The slides were then washed, wet mounted, and examined under a fluorescence microscope. For diaminobenzidine (DAB; Sigma) staining, rat anti-Mac-1 antibody 1:200 (Pharmingen) was used as the primary antibody, followed by a horseradish peroxidase (HRP)-labeled goat anti-rat IgG as the secondary antibody. Staining was visualized with DAB, and slides were washed, dehydrated, cleared in xylene, and mounted. For the in vitro study, cells cultured on chamber slides were fixed with 4% paraformaldehyde in PBS and subjected to immunofluorescence staining. Rabbit anti-GFAP antibody 1:1,000 (Dako) was used as the primary antibody, followed by FITC-conjugated goat anti-rabbit IgG as the secondary antibody. The cells were counterstained with Hoechst 33258 to identify nuclei.

Quantitative Analysis

Images were obtained by fluorescence microscopy (Axioskop 2 plus; Carl Zeiss Co., Ltd., Tokyo, Japan). For quantification of connective tissue scar (CTS) formation in vivo, five representative axial sections, 1.0 mm and 0.5 mm rostral to the lesion epicenter, at the lesion epicenter, and 0.5 mm and 1.0 mm caudal to the lesion epicenter were selected from a 4-mm length of cord, centered over the impact site, and the CTS area was measured using NIH Image software in H&E-stained sections and calculated as a percentage of the total axial area. To evaluate astrogliosis, five representative axial sections were selected as described above, and six regions in each section were captured randomly at ×200 magnification by confocal microscopy (LSM510; Carl Zeiss Co., Ltd.). The glial fibrillary acidic protein (GFAP)/BrdU double-positive cells in each region were counted by three investigators in a blinded fashion, and the density of each section (number of GFAP/BrdU double-positive cells per total axial area) was calculated. To quantify the proportion of the lesion that was Mac-1 immunolabeled, five representative midsagittal sections (3 mm long) were selected, and the immunoreactive area was measured with the MCID system (Imaging Research, Inc., Troonto, Ontario, Canada).

Western Blot Analysis

At 12 hr after the injury, spinal cord tissue of the lesion epicenter (6 mm long) was dissected from the mice (four animals per group and four sham-operated animals), homogenized in MAPK lysis buffer containing protease inhibitor, and after sonication centrifuged at 15,000 rpm. Protein from the supernatant of each sample was separated by 10% SDS-PAGE and transferred to polyvinylidene difluoride membranes by electrophoresis. The membranes were blocked for 1 hr at room temperature in TBST buffer containing 4% nonfat milk, NaCl (150 mM), and 0.05% Tween 20. The blots were then incubated with either primary polyclonal rabbit anti-stat3 antibody, rabbit antiphospho-stat3 antibody 1:500 (Cell Signaling Technology, Beverly, MA), mouse anti-α-tubulin antibody 1:500, or rabbit anti IL-6Rα antibody 1:200 (Santa Cruz Biotechonology, Santa Cruz, CA), followed by a secondary HRP-conjugated anti-rabbit or mouse IgG antibody. The blots were visualized with the ECL Blotting Analysis System (Amersham, Arlington Heights, IL).

Statistical Analysis

Values are reported as means ± SEM. Differences in all tests except for the rearing score analysis were analyzed for statistical significance by the unpaired Student's *t*-test. SCANET rearing scores were compared between groups by ANOVA with the post hoc Fisher's exact test. In all statistical analyses, significance was accepted at $P = .05$.

RESULTS

Effect of MR16-1 on Neural Stem/Progenitor Cells In Vitro

We investigated the effect of IL-6 signaling and MR16-1 on NSPC differentiation in vitro by performing the differentiation assay on adult spinal cord-derived neural precursor cells that had been expanded in a floating culture according to a previously reported method (Reynolds and Weiss, 1992; Shimazaki et al., 2001). Approximately 47.1% of the control NSPCs cultured in medium alone differentiated into astrocytes (Fig. 1A1,B). After addition of IL-6 and sIL-6R to induce gp130-mediated signaling (Taga et al., 1989; Tamura et al., 1993), NSPC differentiation into astrocytes was enhanced, and there was obvious extension of GFAP-positive processes (Fig. 1A2,B). By contrast, addition of MR16-1 to IL-6 plus sIL-6R inhibited the effect of IL-6 plus sIL-6R on astrocytic differentiation (Fig. 1A3), and there was a significant decrease in GFAP-positive cells as a percentage of total live cells in the MR16-1 group compared with the IL-6 plus sIL-6R-alone-treated group (mean value of 43.2% ± 2.8% in the MR16-1 group compared with 64.9% ± 3.5% in the IL-6 plus sIL-6R group; Fig. 1B). There was no significant difference in the number of total live cells between these two groups. These results indicate that the astrocytic differentiation-promoting effect of the IL-6 signal was sufficiently blocked by MR16-1 in vitro.

Histological Changes in Mice After SCI

Two weeks after the SCI, there was no cavitation at the lesion epicenter, but the central gray matter had been completely replaced by CTS in both the control group and the MR16-1 groups (Fig. 2). Single or double immunostaining was then performed to determine composition of the cells at the lesion site. Mac-1-positive inflammatory cells were observed mainly in the scar area (Fig. 2H,I), and Hu-positive neurons were found to remain only in the spared white matter (Fig. 2E,F) compared with uninjured mice (Fig. 2D,G). On the other hand, there were few GFAP-positive cells within the central lesion area, and it was surrounded by GFAP-positive astrocytes in both the axial and the sagittal sections (Fig. 3). We found that the area of the CTS was essentially GFAP negative. Interestingly, the CTS area was smaller in the MR16-1 group (Fig. 3B,D) than in the control group (Fig. 3A,C). Double immunostaining with GFAP and BrdU revealed BrdU in the nuclei of the GFAP-positive cells, indicating that they had divided after the SCI, and they were concluded to be reactive astrocytes.

To determine whether administration of MR16-1 suppressed astrogliosis after SCI, we counted the numbers of GFAP and BrdU double-positive cells at the epicenter and 0.5 and 1.0 mm rostral and caudal to the epicenter (Fig. 4). Representative confocal images of the lesioned area under higher magnification are shown in Figure 4A (control group) and 4B (MR16-1 group). In the MR16-1 group, there were significantly fewer GFAP and BrdU double-positive cells than in the control group (mean of 85.1 ± 2.5 cells/mm^2 in the control group compared with 63.3 ± 9.3 cells/mm^2 in the MR16-1 group; Fig. 4C).

Western Blotting

We confirmed the significantly increased expression of the IL-6 receptor in the injured spinal cord by Western blot analysis. In the intact spinal cord of sham-operated mice (in which only laminectomy was performed), the expression level of the IL-6 receptor was very low. However, the expression level had increased by nearly eightfold at 12 hr after the injury (Fig. 5A,C). To investigate whether the decrease in reactive astrocytes was due to blockade of the IL-6 signal cascade, we performed an analysis of both the total and the phosphorylated forms of the signal transducer and activator of transcription 3 (STAT3), a principal part of the IL-6 family signal cascade. Initiation of IL-6 signaling occurs when IL-6 binds to the IL-6R, which leads to association with gp130, and this receptor complex leads to activation of gp130-associated tyrosine kinases (JAK kinases). JAK activation then leads to tyrosine phosphorylation of STATs (Taga and Kishimoto, 1997; Van Wagoner and Benveniste, 1999; Ohtani et al., 2000). Upon phosphorylation, STAT3 proteins dimerize and translocate to the nucleus, where they bind to elements in the promoter of GFAP genes (Bonni et al., 1997), so quantification of phosphorylated STAT3 is an adequate index of the extent of IL-6 signaling. Administration of MR16-1 decreased the expression of phosphorylated STAT3 compared with the control group (Fig. 5B), and there was a significant difference in the ratio of phosphorylated to total STAT3 expression between the control group and the MR16-1 group (Fig. 5D). These findings suggested that the intraperitoneally injected MR16-1 actually blocked the IL-6/JAK/STAT3 signaling pathway and suppressed astrogliosis after SCI. However, strictly speaking, the alternative possibility that the observed reduction in the phosphorylated STAT3 level in the MR16-

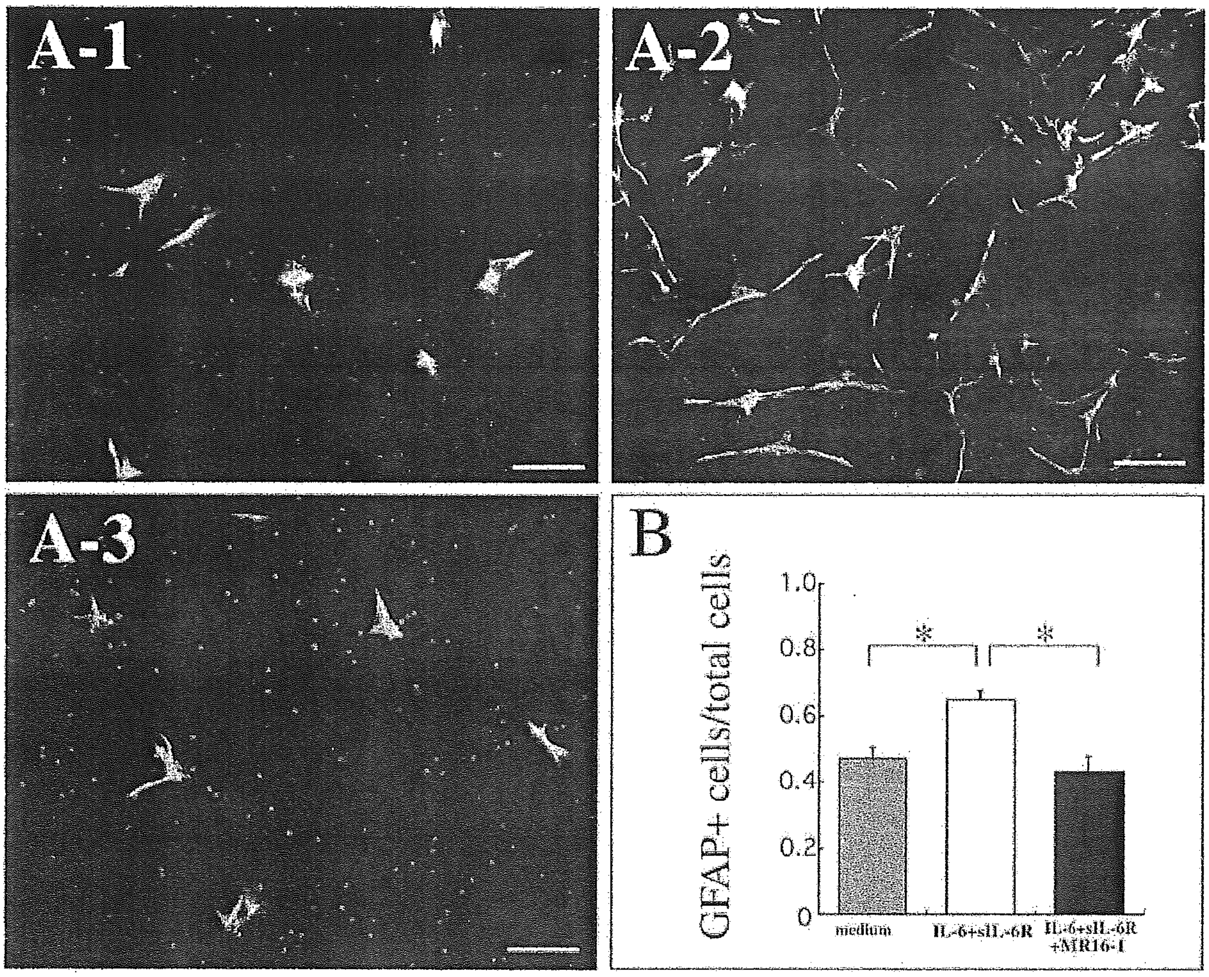

Fig. 1. Effect of the IL-6 signal and MR16-1 on the astrocytic differentiation of NSPCs. **A:** Dissociates of neural progenitor cells were cultured for 3 days with medium alone (A1), IL-6 and soluble IL-6 receptor at 20 ng/ml (A2), and IL-6 and soluble IL-6 receptor plus MR16-1 at 20 μg/ml (A3) and then subjected to immunofluorescence staining for GFAP (green) and Hoechst 33258 (blue). **B:** The number of GFAP-positive cells was calculated as a percentage of all live cells. Values are means ± SEM. *$P < .05$; two-tailed t-test (n = 3). Scale bars = 50 μm.

1-treated group resulted from suppression of astrogliosis by some unknown mechanisms cannot be excluded.

MR16-1 Suppressed the Infiltration by Inflammatory Cells After SCI

In addition to regulation of the astrocytic differentiation of NSPCs, IL-6 plays critical roles as a proinflammatory cytokine that activates macrophages and induces inflammatory cell chemotaxis and fibroblast proliferation (Romano et al., 1997; Van Wagoner and Benveniste, 1999; Tuna et al., 2001). To determine the antiinflammatory effect of MR16-1, we therefore performed immunolabeling of Mac-1-positive cells in sagittal sections at the lesion epicenter. Fewer Mac-1-positive cells were observed at the lesion epicenter 2 weeks after the injury in the MR16-1 group (Fig. 6A,B), and quantitative analysis showed statistically significant differences Mac-1-immunolabeled area in the MR-16 group and in the control group (mean of 5.6% ± 1.0% in the MR16-1 group, compared with 15.1% ± 1.2% in the control group; Fig. 6C). We also measured the area of the CTS after SCI using NIH Image software in H&E-stained serial sections and found that the area of the scar at the lesion epicenter 2 weeks after injury was significantly smaller in the MR16-1 mice (mean 47.4% ± 1.3% in the MR16-1 group compared with 64.5% ± 2.7% in the control group; Fig. 6D). These results indicate that administration of MR16-1 attenuated the inflammatory responses following injury in vivo.

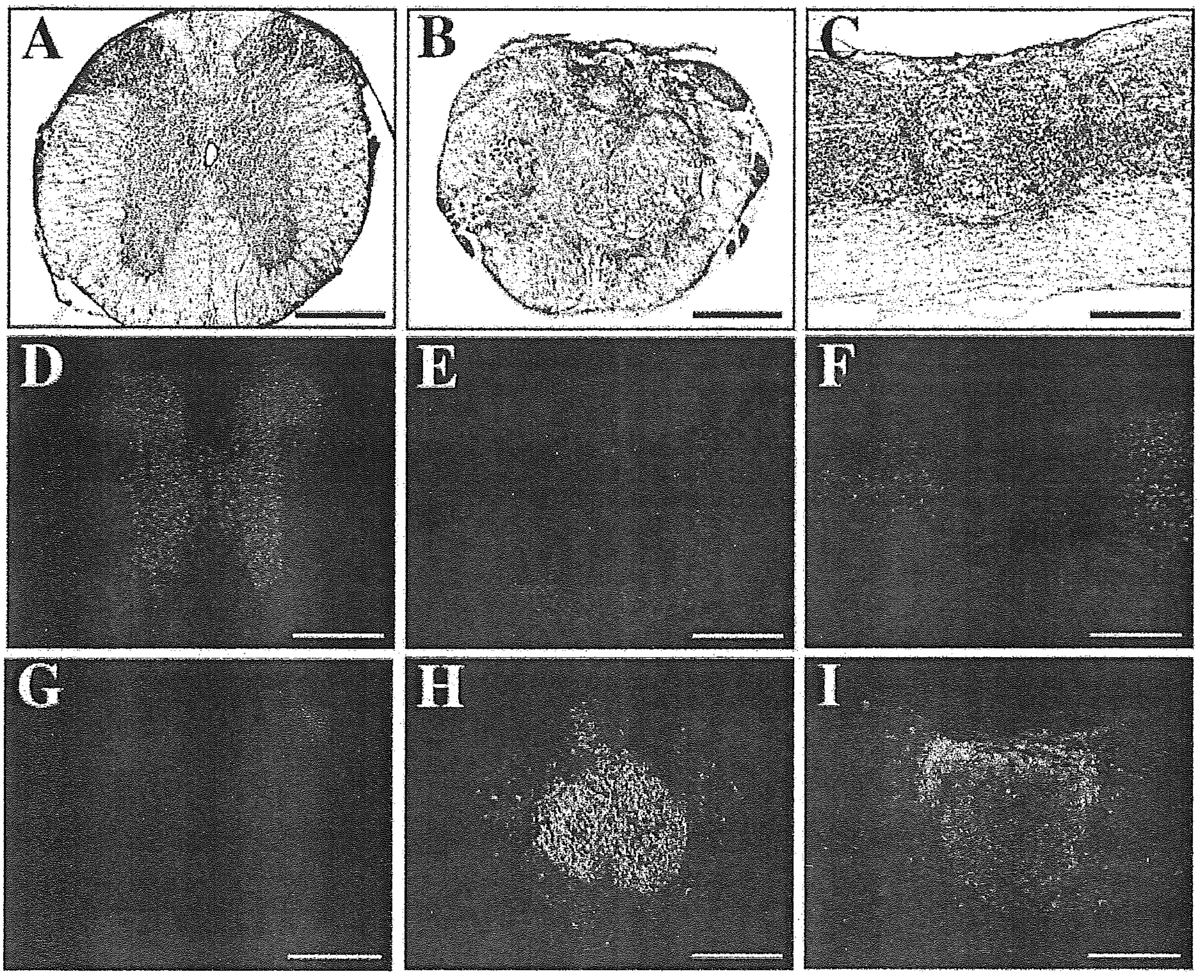

Fig. 2. Photomicrographs of representative immunohistochemistry and H&E-stained sections from the lesion epicenter 2 weeks after injury obtained from the MR16-1 group (B,C,E,F,H,I) and normal mice (A,D,G). **A–C:** H&E staining showed that the normal gray matter in the lesion epicenter had been completely replaced by a connective tissue scar. **D–F:** Distribution of Hu-immunoreactive cells (red) in normal and injured mice. The central lesion area was devoid of Hu-positive neurons. **G–I:** Mac-1 (CD11b)-immunoreactive cells were almost negative in the normal axial section (G), but they were aggregated mainly in the connective tissue scar area in injured spinal cord (H,I). A, B, D, E, G, and H, axial sections; C, F, and I, sagittal sections. Scale bars = 400 μm.

Behavioral Recovery

Given the histopathological improvements, such as the decreased astrogliosis and inflammatory cell infiltration, we investigated whether the histological changes were associated with better functional recovery by using three different behavioral tests. The mice in both the MR-16 group and the control group showed flaccid paralysis with no or little hindlimb movement throughout the first week after SCI, and this was followed by some recovery of hindlimb movement. To assess such functional recovery, we first examined a standardized open-field measure of locomotor function after the SCI, the BBB score, in which 21 is normal function and 0 is bilateral total paralysis of the hindlimbs. When BBB scoring is applied to mice, the size and speed of the hindpaws make it difficult to assign a precise score if the score exceeds 13 points (Ma et al., 2001), but that was not a problem in this study, because none of the mice had scores over 13 points (Jakeman et al., 2000). By 6 weeks after the injury, mice in the MR16-1 group had a significantly higher motor score (9.1 ± 0.5) than the control animals (6.4 ± 0.7), and the differences between the two groups 5 and 6 weeks after the injury were statistically significant (Fig. 7A). In the BBB score, 9 points represents the ability for hindlimb weight bearing. Even in mice, the difference of 8 points and 9 points was clearly detectable, because it was obvious whether they could bear weight or not.

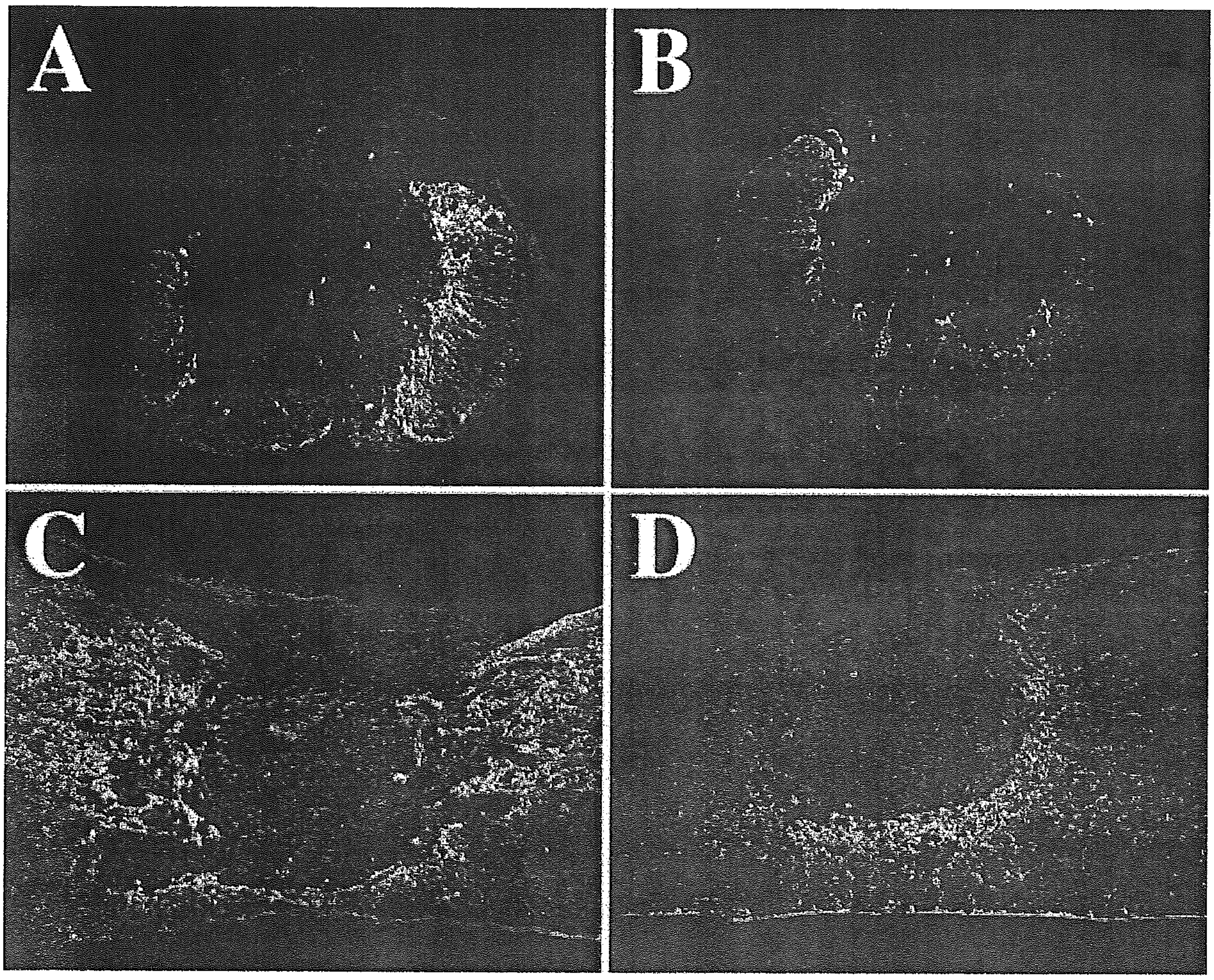

Fig. 3. Sections from the lesion epicenter of control mice (**A**,**C**) and MR16-1-treated mice (**B**,**D**) were counterstained with GFAP (green) and BrdU (red). The connective tissue scar area was almost completely GFAP negative but was surrounded with GFAP-positive astrocytes. This area in MR16-1-treated mice was smaller and astrogliosis around the central lesion was suppressed moderately compared with the control mice. A, B, axial sections; C, D, sagittal sections.

We then used a second assay employing SCANET, an automated motion-analysis system for measuring spontaneous motor activity (Shimosato and Ohkuma, 2000; Mikami et al., 2002), which is capable of assessing not only horizontal but also vertical movement. Vertical movement is an adequate index for assessment of locomotor function in spinal cord-injured mice. Mikami et al. (2002) even reported a statistically significant positive correlation between the RG score and the BBB Scale score. The vertical movement analysis revealed that 12 of the 15 mice in the MR16-1 group were able to rear more than once, whereas only 3 of the 15 mice were able to do so in the control group. The difference between the two groups was significant according to Fisher's exact probability test ($P < .05$). However, there were no significant differences in horizontal movements between the groups.

We performed the Rota-rod treadmill test to assess recovery of forelimb–hindlimb coordination. At low speed (5 rpm), there were statistically significant differences between the groups in average and maximum retention time in three trials at 5 and 6 weeks after the injury (Fig. 6B), but no differences were demonstrated at the middle speed (10 rpm) or high speed (15 rpm). These findings indicated that the recovery of forelimb–hindlimb coordination was poor even in the MR16-1 group, and they were consistent with the BBB scores, which never exceeded 12 points. In conclusion, MR16-1 group exhibited better functional recovery than the control mice in all three behavioral evaluations.

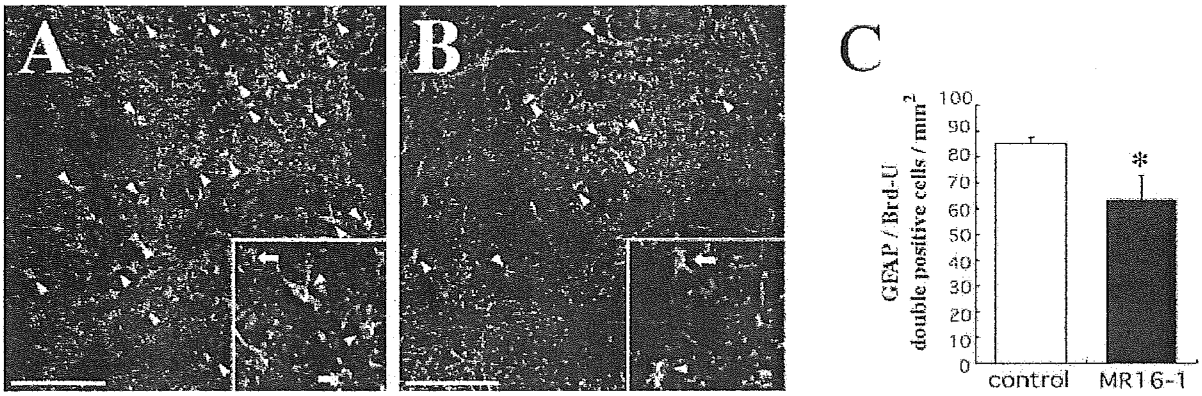

Fig. 4. MR16-1 suppressed the astrogliosis after SCI. **A,B:** Immunofluorescence staining for GFAP (green) and BrdU (red) at 2 weeks after the injury. Confocal imaging of the lesioned area with higher magnification in the control group (A) and MR16-1 group (B). **Insets:** Magnified views of A and B. Arrowheads point to a GFAP and BrdU double-positive cell, and the arrows point to GFAP-positive and BrdU-negative cells. **C:** Quantitative analysis of the average density of GFAP and BrdU double-positive cells at the lesion epicenter and 0.5 mm and 1.0 mm rostral and caudal to the epicenter in both groups. Values are means ± SEM. $*P < .05$; two-tailed t-test (n = 4 in the control group; n = 3 in the MR16-1 treated group). Scale bars = 40 μm.

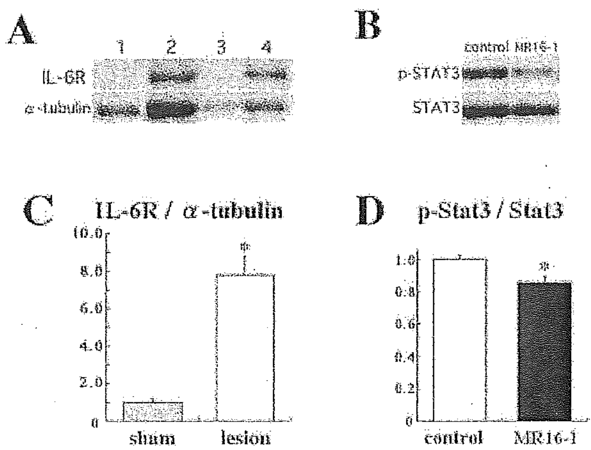

Fig. 5. Western blot analysis. **A,C:** Western blotting of soluble IL-6 receptor in the sham-operated spinal cord (lanes 1, 3) and lesioned spinal cord at 12 hr after the injury (lanes 2, 4). Quantification analysis revealed that the expression of IL-6R was 7.8-fold higher in the lesioned group at 12 hr after the injury compared with that in the sham group (n = 4 per each group). The average expression in the sham group was set as 1.0. $*P < .01$. **B,D:** The phosphorylated-STAT3 expression level in the spinal cord at 12 hr after the injury was quantitatively compared by Western blot analysis. The expression level of phosphorylated STAT3 in the MR16-1-treated group was 85.1% less compared with that in the control group. Values represent means ± SEM of the p-STAT3/STAT3 ratios (n = 4 per each group), with the average ratio in the control group set as 1.0. $*P < .05$.

DISCUSSION

Neutralization of soluble IL-6 receptor (sIL-6R) represents an attractive option for the treatment of several diseases characterized by excessive expression of IL-6, including B-cell neoplasia, rheumatoid arthritis, and autoimmune diseases (Yoshizaki et al., 1989; Takagi et al., 1998; Atreya et al., 2000). In this study, we first showed that the monoclonal anti-IL-6 receptor-α antibody MR16-1 blocked the IL-6 signaling that induced NSPCs to differentiate into astrocytes in vitro. Bonni et al. (1997) observed that activation of the gp130 signaling pathway selectively enhanced the differentiation of embryonic cerebral cortical precursor cells toward astrocytes, and we confirmed very similar effects of IL-6 signaling on NSPCs harvested from the spinal cord of adult mice.

Johansson et al. (1999) demonstrated that the endogenous NSPCs of adult spinal cord proliferate rapidly and differentiate exclusively into astrocytes in response to injury. Although the precise mechanism of this restrictive differentiation of NSPCs remains to be elucidated, activation of IL-6 signaling could be one of the major contributions of such selective astrocytic differentiation after SCI. IL-6 expression increases dramatically during the acute phase of SCI and then declines sharply within a few days (Hostettler and Carlson, 2002; Pan et al., 2002; Nakamura et al., 2003), and we confirmed the increase in sIL-6R (Yan et al., 1992) after SCI by Western blot analysis (Fig. 5A,C). This up-regulation of IL-6 signaling in the acute phase would be closely associated with glial scar formation after SCI (for review see Okano, 2002; Okano et al., 2003). Klein et al. (1997) show a massive reduction in the number of activated GFAP-positive astrocytes when the facial nerve of IL-6-deficient mice was transected, and Brunello et al. (2000) demonstrated massive reactive gliosis with numerous GFAP-immunoreactive astrocytes in all parts of the CNS in uninjured IL-6/sIL-6R double-transgenic mice. Therefore, we hypothesized that the astrogliosis could be suppressed by blocking IL-6 signaling after

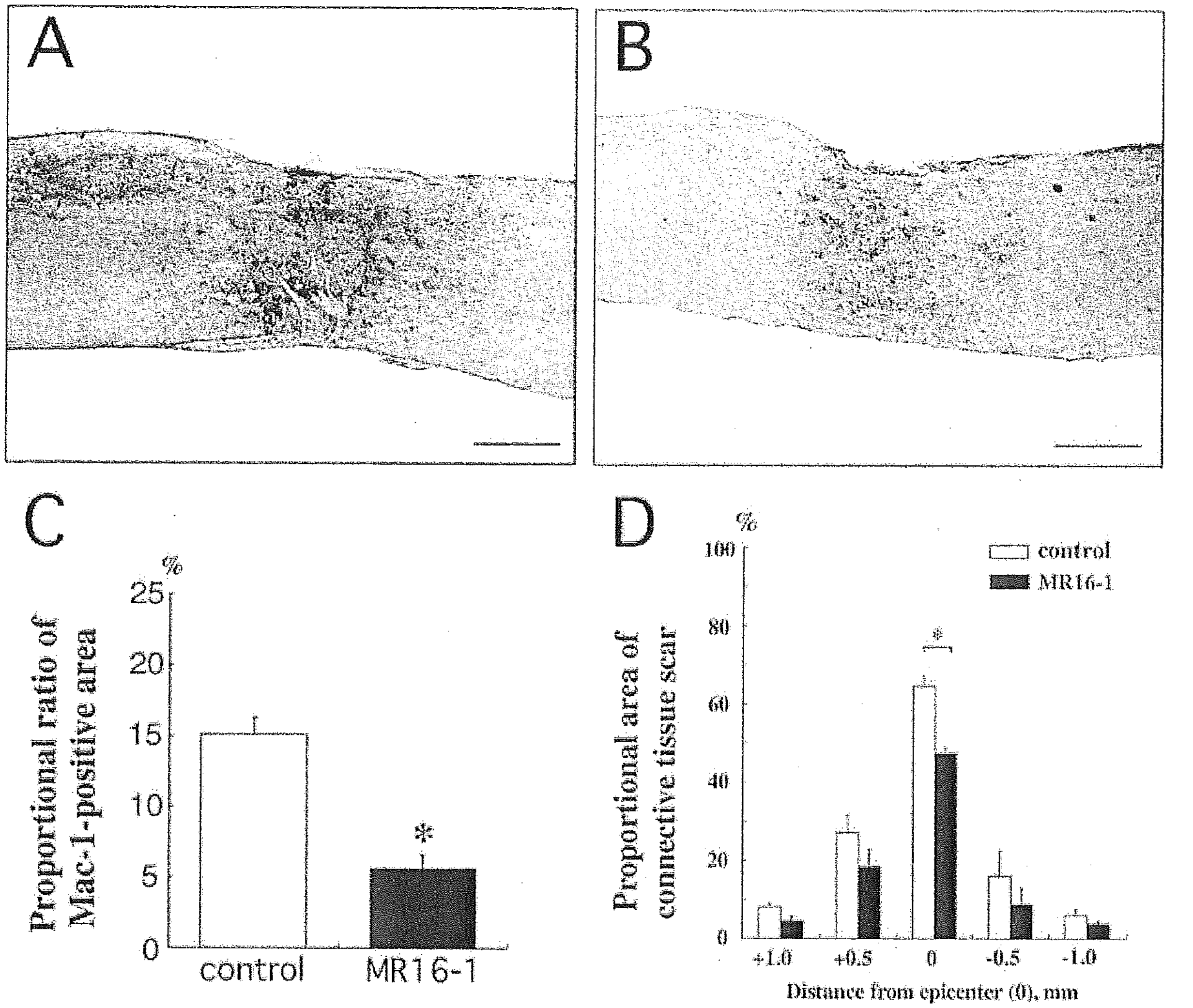

Fig. 6. Inflammatory responses were markedly decreased by MR16-1. **A,B:** Immunolabeling of Mac-1-positive cells in injured spinal cord at 2 weeks after injury. Representative sagittal section at the lesion epicenter from the control group (A) and the M16-1 group (B). **C:** Measurement of the area of Mac-1 immiunoreactivity in 3-mm sagittal sections from both groups. The immunolabeled area was significantly smaller in the MR16-1 group than in the control group. Values are means ± SEM. $*P < .05$; two-tailed t-test (n = 4 in the control group; n = 3 in the MR16-1 group). **D:** The area of the connective tissue scar as a percentage of the total axial area was calculated at the lesion epicenter and 0.5 and 1.0 mm rostral and caudal to the epicenter in both groups. The connective tissue scar area in the epicenter was significantly smaller in the MR16-1 mice. Values are means ± SEM. $*P < .05$; two-tailed t-test (n = 4 per each group). Scale bars = 500 μm.

SCI in vivo. In the present study, we showed a 15% decrease of phosphorylated-STAT3 expression at 12 hr after the injury and a 25% decrease in the number of GFAP and BrdU double-positive cells at 2 weeks after injury with systemic administration of MR16-1, compared with the control animals, suggesting that astrogliosis and IL-6 signaling are closely related. However, the precise mechanism regulating astrogliosis remains to be elucidated. In the present study, we were not able to determine the extent to which endogenous multipotential progenitors or resident astrocytes contributed to the $GFAP^+/BrdU^+$ cells. Kernie et al. (2001), however, reported that a significant amount of the astrogliotic scar formed after an injury is attributable to newly generated astrocytes and not to activation or migration of resident astrocytes.

Glial scar formation is considered a major cause of the poor regeneration after adult CNS after injury. A

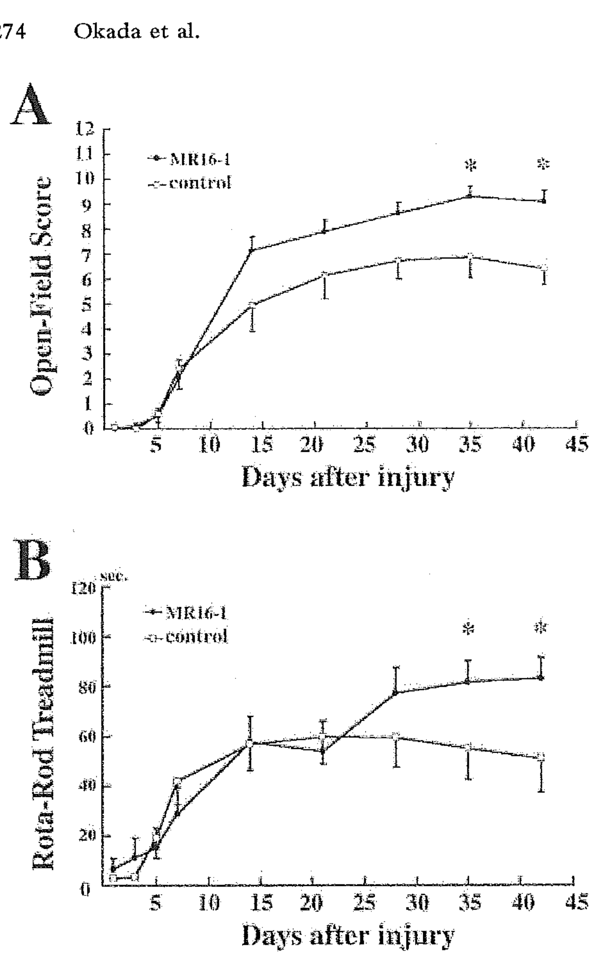

Fig. 7. Effect of MR16-1 on functional recovery. **A:** BBB scores in the control group (n = 15) and MR16-1 group (n = 15) were evaluated over a 6-week period. **B:** Retention time on the rotating rod in the control group (n = 15) and MR16-1 group (n = 15) at a speed of 5 rpm. Squares represent control mice, and circles represent MR16-1-treated mice. Values are means ± SEM. $*P < .05$; two-tailed *t*-test.

recent study reported that glial scars and associated extracellular matrix inhibit axonal regeneration with several molecules, such as chondroitin sulfate proteoglycans, tenascin, brevican, and neurocan (Fawcett and Asher, 1999). Bradbury et al. (2002) also demonstrated that degradation of chondroitin sulfate proteoglycans that are contained in glial scars at injury site with chondroitinase ABC improved functional recovery and promoted regeneration of both ascending sensory projections and descending long tract axons. Thus, modulating astrogliosis is a rational target for treating spinal cord injury and enhancing axonal regeneration, resulting in functional recovery (McGraw et al., 2001). Ridet et al. (2000) reported that suppression of glial scar formation with a 2-Gy dose of radiation after injury also improved functional recovery. In the present study, we demonstrated that administration of MR16-1 promoted functional recovery in three different behavioral evaluations (Fig. 7). Although further investigations are required, one possible explanation for the observed functional recovery is that the suppression of astrogliosis by MR16-1 treatment reduced the expression of glial scar-derived inhibitory molecules against axonal regeneration, which promoted axonal regeneration after injury.

Manipulation of inflammatory responses is another therapeutic strategy for SCI. Although the precise functions and effects of inflammatory cells after injury have not been completely elucidated, previous studies have suggested that inflammatory responses spread the damage to surrounding tissue, induce apoptotic cell death, and impair spontaneous regeneration and functional recovery (Carlson et al., 1998; Popovich and Jones, 2003). Several approaches to protecting the injured spinal cord from secondary pathological processes, such as the antiinflammatory cytokine IL-10, erythropoietin, matrix metalloprotease inhibitor, and methylprednisolone, have been assessed and been demonstrated to be effective, even in terms of functional recovery (Bracken et al., 1997; Bethea et al., 1999; Gorio et al., 2002; Nobel et al., 2002). IL-6 is one of the principal proinflammatory cytokines; it plays roles in regulating various steps in inflammatory reactions, i.e., activation and infiltration by neutrophils, monocytes, macrophages, and lymphocytes (Van Wagoner and Benveniste, 1999; Leskovar et al., 2000). The number of inflammatory cells is significantly correlated with the amount of tissue damage at each level (Carlson et al., 1998), and the size of the CTS, which is the characteristic lesion of contusive SCI in mice, as opposed to central cavitation in rats, correlates with the severity of the injury (Ma et al., 2001). We tested, based on these studies, our hypothesis that MR16-1 would suppress the inflammatory response after injury by assessing the extent of Mac-1-positive inflammatory cell infiltration and measuring the area of the CTS. The results demonstrated that fewer Mac-1-positive cells infiltrated both the gray and the white matter and that the CTS area at the lesion epicenter was significantly smaller in the MR16-1 group than in the control group (Fig. 6). This modulation of the inflammatory response after injury by administration of MR16-1 probably attenuated the tissue damage and secondary neural destruction and caused the functional recovery demonstrated in the present study (Fig. 7). Our findings are consistent with the results of previous studies suggesting that administration of proinflammatory cytokines at lesion sites 1 day after an injury increases the recruitment and activation of macrophages, neutrophils, and microglial cells (Klusman and Schwab, 1997) and that delivery of IL-6/sIL-6R fusion protein to injury sites induces a sixfold increase in neutrophils and a twofold increase of macrophages and microglial cells (Lacroix et al., 2002).

By contrast, IL-6 exerts multiple effects in the CNS, and several experiments have shown the neuronal protective and outgrowth effects of IL-6 signaling. For example, Marz et al. (1998) showed that IL-6 signaling enhances neuronal survival in rat sympathetic neurons, and Hirota et al. (1996) observed accelerated regeneration of the axotomized hypoglossal nerve in transgenic mice constitutively expressing IL-6 and IL-6R. Administration of IL-6 to animals with cerebral ischemia reduced tissue damage and prevented learning disabilities in vivo (Matsuda et al., 1996; Loddick et al., 1998). In SCI, however, delivery of IL-6/sIL-6R fusion protein (hyper-IL-6) to the lesion site induced a fourfold decrease in axonal outgrowth, which indicated that the neurotrophic effects of IL-6 were overwhelmed by its proinflammatory features in vivo (Lacroix et al., 2002). These clear differences in IL-6 effect may depend on the level and timing of its expression. Although the role of IL-6 signaling seemed to be complex and well regulated in accordance with the physiopathology, we wish to emphasize the neurotoxic effect of IL-6, at least in the acute phase after SCI. We also confirmed by ELISA (data not shown) that the half-life of MR16-1 is about 3 days in injured mice, so the kinetics of MR16-1 would produce an ideal effect, because it suppresses excess IL-6 signaling only in the acute phase and dose not interfere the neuroprotective effect in the subacute and chronic phases.

A critical merit of this sIL-6R antibody is that humanized antibody to human IL-6R (MRA; Atlizumab) has already been reshaped (Sato et al., 1993), and its therapeutic efficacy has been confirmed in clinical trials in several diseases, including rheumatoid arthritis, Castleman's disease, and multiple myeloma (Sato et al., 1993; Nishimoto et al., 2000; Choy et al., 2002). The Phase II clinical trial in rheumatoid arthritis has already been completed in Japan and Europe, and safety, tolerability, antigenicity, pharmacokinetics, and efficacy have been demonstrated. Although the data reported here are preliminary, they suggest that blockage of IL-6 signaling may be beneficial in patients with acute SCI. In summary, the results of this study show that a single dose of anti-mouse IL-6R monoclonal antibody enhances functional recovery after SCI in adult mice, probably by attenuating inflammatory response, secondary tissue damage, and astrogliosis.

ACKNOWLEDGMENTS

We thank Drs. K. Shiba and T. Ueta (Spina Cord Injury Center, Fukuoka, Japan) for their continuous encouragement and valuable discussions. This work was supported by grants from the Japanese Ministry of Education, Culture, Sports, Science and Technology and the Japan Science and Technology Corporation (CREST) to H.O., and a Grant-in-Aid for the 21st Century COE (Center of Excellence) program to Keio University from the Japanese Ministry of Education, Culture, Sports, Science and Technology.

REFERENCES

Atreya R, Mudter J, Finotto S, Mullberg J, Jostock T, Wirtz S, Schutz M, Bartsch B, Holtmann M, Becker C, Strand D, Czaja J, Schlaak JF, Lehr HA, Autschbach F, Schurmann G, Nishimoto N, Yoshizaki K, Ito H, Kishimoto T, Galle PR, Rose-John S, Neurath MF. 2000. Blockade of interleukin 6 trans signaling suppresses T-cell resistance against apoptosis in chronic intestinal inflammation: evidence in crohn disease and experimental colitis in vivo. Nat Med 6:583–588.

Basso DM, Beattie MS, Bresnahan JC. 1996. Graded histological and locomotor outcomes after spinal cord contusion using the NYU weight-drop device versus transection. Exp Neurol 139:244–256.

Bethea JR, Nagashima H, Acosta MC, Briceno C, Gomez F, Marcillo AE, Loor K, Green J, Dietrich WD. 1999. Systemically administered interleukin-10 reduces tumor necrosis factor-alpha production and significantly improves functional recovery following traumatic spinal cord injury in rats. J Neurotrauma 16:851–863.

Bjorklund A, Lindvall O. 2000. Self-repair in the brain. Nature 405:892–895.

Bonni A, Sun Y, Nadal-Vicens M, Bhatt A, Frank DA, Rozovsky I, Stahl N, Yancopoulos GD, Greenberg ME. 1997. Regulation of gliogenesis in the central nervous system by the JAK-STAT signaling pathway. Science 278:477–483.

Bracken MB, Shepard MJ, Holford TR, Leo-Summers L, Aldrich EF, Fazl M, Fehlings M, Herr DL, Hitchon PW, Marshall LF, Nockels RP, Pascale V, Perot PL Jr, Piepmeier J, Sonntag VK, Wagner F, Wilberger JE, Winn HR, Young W. 1997. Administration of methylprednisolone for 24 or 48 hr or tirilazad mesylate for 48 hr in the treatment of acute spinal cord injury. Results of the Third National Acute Spinal Cord Injury Randomized Controlled Trial. National Acute Spinal Cord Injury Study. JAMA 277:1597–1604.

Bradbury EJ, Moon LD, Popat RJ, King VR, Bennett GS, Patel PN, Fawcett JW, McMahon SB. 2002. Chondroitinase ABC promotes functional recovery after spinal cord injury. Nature 416:636–640.

Brunello AG, Weissenberger J, Kappeler A, Vallan C, Peters M, Rose-John S, Weis J. 2000. Astrocytic alterations in interleukin-6/soluble interleukin-6 receptor alpha double-transgenic mice. Am J Pathol 157: 1485–1493.

Carlson SL, Parrish ME, Springer JE, Doty K, Dossett L. 1998. Acute inflammatory response in spinal cord following impact injury. Exp Neurol 151:77–88.

Choy EH, Isenberg DA, Garrood T, Farrow S, Ioannou Y, Bird H, Cheung N, Williams B, Hazleman B, Price R, Yoshizaki K, Nishimoto N, Kishimoto T, Panayi GS. 2002. Therapeutic benefit of blocking interleukin-6 activity with an anti-interleukin-6 receptor monoclonal antibody in rheumatoid arthritis: a randomized, double-blind, placebo-controlled, dose-escalation trial. Arthritis Rheum 46:3143–3150.

David S, Lacroix S. 2003. Molecular approaches to spinal cord repair. Annu Rev Neurosci 26:411–440.

Fawcett JW, Asher RA. 1999. The glial scar and central nervous system repair. Brain Res Bull 49:377–391.

Gorio A, Gokmen N, Erbayraktar S, Yilmaz O, Madaschi L, Cichetti C, Di Giulio AM, Vardar E, Cerami A, Brines M. 2002. Recombinant human erythropoietin counteracts secondary injury and markedly enhances neurological recovery from experimental spinal cord trauma. Proc Natl Acad Sci USA 99:9450–9455.

Gruner JA. 1992. A monitored contusion model of spinal cord injury in the rat. J Neurotrauma 9:123–128.

Hirota H, Kiyama H, Kishimoto T, Taga T. 1996. Accelerated nerve regeneration in mice by upregulated expression of interleukin (IL) 6 and IL-6 receptor after trauma. J Exp Med 183:2627–2634.

Horner PJ, Power AE, Kempermann G, Kuhn HG, Palmer TD, Winkler J, Thal LJ, Gage FH. 2000. Proliferation and differentiation of progenitor cells throughout the intact adult rat spinal cord. J Neurosci 20:2218–2228.

Hostettler ME, Carlson SL. 2002. PAF antagonist treatment reduces pro-inflammatory cytokine mRNA after spinal cord injury. Neuroreport 13:21–24.

Jakeman LB, Guan Z, Wei P, Ponnappan R, Dzwonczyk R, Popovich PG, Stokes BT. 2000. Traumatic spinal cord injury produced by controlled contusion in mouse. J Neurotrauma 17:299–319.

Johansson CB, Momma S, Clarke DL, Risling M, Lendahl U, Frisen J. 1999. Identification of a neural stem cell in the adult mammalian central nervous system. Cell 96:25–34.

Katsume A, Saito H, Yamada Y, Yorozu K, Ueda O, Akamatsu KI, Nishimoto N, Kishimoto T, Yoshizaki K, Ohsugi Y. 2002. Anti-interleukin 6 (IL-6) receptor antibody suppresses castleman's disease like symptoms emerged in IL-6 transgenic mice. Cytokine 20:304–311.

Kernie SG, Erwin TM, Parada LF. 2001. Brain remodeling due to neuronal and astrocytic proliferation after controlled cortical injury in mice. J Neurosci Res 66:317–326.

Klein MA, Moller JC, Jones LL, Bluethmann H, Kreutzberg GW, Raivich G. 1997. Impaired neuroglial activation in interleukin-6 deficient mice. Glia 19:227–233.

Klusman I, Schwab ME. 1997. Effects of pro-inflammatory cytokines in experimental spinal cord injury. Brain Res 762:173–184.

Kuhn PL, Wrathall JR. 1998. A mouse model of graded contusive spinal cord injury. J Neurotrauma 15:125–140.

Lacroix S, Chang L, Rose-John S, Tuszynski MH. 2003. Delivery of hyper-interleukin-6 to the injured spinal cord increases neutrophil and macrophage infiltration and inhibits axonal growth. J Comp Neurol 454:213–228.

Leskovar A, Moriarty LJ, Turek JJ, Schoenlein IA, Borgens RB. 2000. The macrophage in acute neural injury: changes in cell numbers over time and levels of cytokine production in mammalian central and peripheral nervous systems. J Exp Biol 203:1783–1795.

Loddick SA, Turnbull AV, Rothwell NJ. 1998. Cerebral interleukin-6 is neuroprotective during permanent focal cerebral ischemia in the rat. J Cereb Blood Flow Metab 18:176–179.

Ma M, Basso DM, Walters P, Stokes BT, Jakeman LB. 2001. Behavioral and histological outcomes following graded spinal cord contusion injury in the C57Bl/6 mouse. Exp Neurol 169:239–254.

Marz P, Cheng JG, Gadient RA, Patterson PH, Stoyan T, Otten U, Rose-John S. 1998. Sympathetic neurons can produce and respond to interleukin 6. Proc Natl Acad Sci USA 95:3251–3256.

Matsuda S, Wen TC, Morita F, Otsuka H, Igase K, Yoshimura H, Sakanaka M. 1996. Interleukin-6 prevents ischemia-induced learning disability and neuronal and synaptic loss in gerbils. Neurosci Lett 204:109–112.

McGraw J, Hiebert GW, Steeves JD. 2001. Modulating astrogliosis after neurotrauma. J Neurosci Res 63:109–115.

Meima L, Moran P, Matthews W, Caras IW. 1997. Lerk2 (ephrin-B1) is a collapsing factor for a subset of cortical growth cones and acts by a mechanism different from AL-1 (ephrin-A5). Mol Cell Neurosci 9:314–328.

Mikami Y, Toda M, Watanabe M, Nakamura M, Toyama Y, Kawakami Y. 2002. A simple and reliable behavioral analysis of locomotor function after spinal cord injury in mice. Technical note. J Neurosurg 97:142–147.

Nakamura M, Houghtling RA, McArthur L, Bayer BM, Bregman BS. 2003. Difference in cytokine gene expression profile between acute and secondary injury in adult rat spinal cord. Ex Neurol 184:313–325.

Nakashima K, Yanagisawa M, Arakawa H, Kimura N, Hisatsune T, Kawabata M, Miyazono K, Taga T. 1999. Synergistic signaling in fetal brain by STAT3-Smad1 complex bridged by p300. Science 284:479–482.

Nishimoto N, Sasai M, Shima Y, Nakagawa M, Matsumoto T, Shirai T, Kishimoto T, Yoshizaki K. 2000. Improvement in Castleman's disease by humanized anti-interleukin-6 receptor antibody therapy. Blood 95:56–61.

Noble LJ, Donovan F, Igarashi T, Goussev S, Werb Z. 2002. Matrix metalloproteinases limit functional recovery after spinal cord injury by modulation of early vascular events. J Neurosci 22:7526–7535.

Ogura H, Matsumoto M, Mikoshiba K. 2001. Motor discoordination in mutant mice heterozygous for the type 1 inositol 1,4,5-trisphosphate receptor. Behav Brain Res 122:215–219.

Ohtani T, Ishihara K, Atsumi T, Nishida K, Kaneko Y, Miyata T, Itoh S, Narimatsu M, Maeda H, Fukada T, Itoh M, Okano H, Hibi M, Hirano T. 2000. Dissection of signaling cascades through gp130 in vivo: reciprocal roles for STAT3- and SHP2-mediated signals in immune responses. Immunity 12:95–105.

Okano H. 2002. Stem cell biology of the central nervous system. J Neurosci Res 69:698–707.

Okano H, Ogawa Y, Nakamura M, kaneko S, Iwanami A, Toyama Y. 2003. Transplantation of neural stem cells into the spinal cord after injury. Semin Cell Dev Biol 14:191–198.

Okazaki M, Yamada Y, Nishimoto N, Yoshizaki K, Mihara M. 2002. Characterization of anti-mouse interleukin-6 receptor antibody. Immunol Lett 84:231–240.

Pan JZ, Ni L, Sodhi A, Aguanno A, Young W, Hart RP. 2002. Cytokine activity contributes to induction of inflammatory cytokine mRNAs in spinal cord following contusion. J Neurosci Res 68:315–322.

Popovich PG, Jones TB. 2003. Manipulating neuroinflammatory reactions in the injured spinal cord: back to basics. Trends Pharmacol Sci 24:13–17.

Reynolds BA, Tetzlaff W, Weiss S. 1992. A multipotent EGF-responsive striatal embryonic progenitor cell produces neurons and astrocytes. J Neurosci 12:4565–4574.

Ridet JL, Pencalet P, Belcram M, Giraudeau B, Chastang C, Philippon J, Mallet J, Privat A, Schwartz L. 2000. Effects of spinal cord X-irradiation on the recovery of paraplegic rats. Exp Neurol 161:1–14.

Romano M, Sironi M, Toniatti C, Polentarutti N, Fruscella P, Ghezzi P, Faggioni R, Luini W, van Hinsbergh V, Sozzani S, Bussolino F, Poli V, Ciliberto G, Mantovani A. 1997. Role of IL-6 and its soluble receptor in induction of chemokines and leukocyte recruitment. Immunity 6:315–325.

Sato K, Tsuchiya M, Saldanha J, Koishihara Y, Ohsugi Y, Kishimoto T, Bendig MM. 1993. Reshaping a human antibody to inhibit the interleukin 6-dependent tumor cell growth. Cancer Res 53:851–856.

Shimazaki T, Shingo T, Weiss S. 2001. The ciliary neurotrophic factor/leukemia inhibitory factor/gp130 receptor complex operates in the maintenance of mammalian forebrain neural stem cells. J Neurosci 21:7642–7653.

Shimosato K, Ohkuma S. 2000. Simultaneous monitoring of conditioned place preference and locomotor sensitization following repeated administration of cocaine and methamphetamine. Pharmacol Biochem Behav 66:285–292.

Taga T, Kishimoto T. 1997. Gp130 and the interleukin-6 family of cytokines. Annu Rev Immunol 15:797–819.

Taga T, Hibi M, Hirata Y, Yamasaki K, Yasukawa K, Matsuda T, Hirano T, Kishimoto T. 1989. Interleukin-6 triggers the association of its receptor with a possible signal transducer, gp130. Cell 58:573–581.

Takagi N, Mihara M, Moriya Y, Nishimoto N, Yoshizaki K, Kishimoto T, Takeda Y, Ohsugi Y. 1998. Blockage of interleukin-6 receptor ameliorates joint disease in murine collagen-induced arthritis. Arthritis Rheum 41:2117–2121.

Takahashi M, Arai Y, Kurosawa H, Sueyoshi N, Shirai S. 2003. Ependymal cell reactions in spinal cord segments after compression injury in adult rat. J Neuropathol Exp Neurol 62:185–194.

Tamura T, Udagawa N, Takahashi N, Miyaura C, Tanaka S, Yamada Y, Koishihara Y, Ohsugi Y, Kumaki K, Taga T. 1993. Soluble interleukin-6 receptor triggers osteoclast formation by interleukin 6. Proc Natl Acad Sci USA 90:11924–11928.

Tuna M, Polat S, Erman T, Ildan F, Gocer AI, Tuna N, Tamer L, Kaya M, Cetinalp E. 2001. Effect of anti-rat interleukin-6 antibody after spinal cord injury in the rat: inducible nitric oxide synthase expression, sodium- and potassium-activated, magnesium-dependent adenosine-5′-triphosphatase and superoxide dismutase activation, and ultrastructural changes. J Neurosurg 95:64–73.

Van Wagoner NJ, Benveniste EN. 1999. Interleukin-6 expression and regulation in astrocytes. J Neuroimmunol 100:124–139.

Yan HQ, Banos MA, Herregodts P, Hooghe R, Hooghe-Peters EL. 1992. Expression of interleukin (IL)-1 beta, IL-6 and their respective receptors in the normal rat brain and after injury. Eur J Immunol 22:2963–7291.

ELSEVIER

MCN Molecular and Cellular Neuroscience

www.elsevier.com/locate/ymcne
Mol. Cell. Neurosci. 26 (2004) 258–270

Downregulation of STAT3 activation is required for presumptive rod photoreceptor cells to differentiate in the postnatal retina

Yoko Ozawa,[a,b] Keiko Nakao,[a,c] Takuya Shimazaki,[a,c] Junji Takeda,[d] Shizuo Akira,[e] Katsuhiko Ishihara,[f] Toshio Hirano,[f,g] Yoshihisa Oguchi,[b] and Hideyuki Okano[a,c,*]

[a] *Department of Physiology, Keio University School of Medicine, Shinjuku, Tokyo 160-8582, Japan*
[b] *Department of Ophthalmology, Keio University School of Medicine, Shinjuku, Tokyo 160-8582, Japan*
[c] *Core Research for Evolutional Science and Technology (CREST), Japan Science and Technology Corporation (JST), Honcho, Kawaguchi, Saitama 332-0012, Japan*
[d] *Collaborative Research Center for Advanced Science and Technology and Department of Social and Environmental Medicine, Graduate School of Medicine, Osaka University, Suita, Osaka 565-0871, Japan*
[e] *Department of Host Defense, Research Institute for Microbial Diseases, Osaka University, Suita, Osaka 565-0871, Japan*
[f] *Laboratory of Developmental Immunology, Graduate School of Frontier Biosciences, Osaka University, Suita, Osaka 565-0871, Japan*
[g] *Laboratory for Cytokine Signaling, RIKEN Research Center for Allergy and Immunology, Tsurumi, Yokohama City, Kanagawa 230-0045, Japan*

Received 28 July 2003; revised 10 February 2004; accepted 10 February 2004

Available online 17 April 2004

Ciliary neurotrophic factor (CNTF) has been known to inhibit the differentiation of presumptive rod photoreceptor cells; however, the underlying mechanisms have remained to be elucidated. We demonstrated that STAT3 activation, but not SHP2 activation, is responsible for the CNTF/gp130 signaling that inhibits expression of Rhodopsin and its upstream activator, *crx*, in the retinal explants derived from P0 mice (P0 retinal explants), utilizing STAT3-deficient retina and electroporation of dominant-negative form of STAT3 (STAT3F). We also demonstrated that STAT3 activation in presumptive rod photoreceptor cells at E18.5 is rapidly downregulated at P0, when Rhodopsin expression starts during retinal development. Persistent STAT3 activation in the P0 retinal explants prevented Rhodopsin expression and rapid upregulation of *crx* expression. STAT3-deficient retinas did not exhibit precocious rod photoreceptor cell differentiation as a whole, although they occasionally exhibited precocious upregulation of *crx* mRNA. Thus, we conclude that downregulation of STAT3 activation is required, but insufficient, for rod photoreceptor cell differentiation in the postnatal retina.

Introduction

It is well known that retinal cell differentiation occurs sequentially during the perinatal period, extending from the late embryonic period to the early postnatal period, so that the composition and arrangement of each cell type are well organized within the neural retina (Cepko et al., 1996; Livesey and Cepko, 2001). However, since there are considerable overlaps between the birth dates of the different cell types (Morrow et al., 1998a,b), there must be some regulatory mechanisms that strictly control the timing of differentiation of postmitotic cells. Presumptive rod photoreceptor cells first appear to exit cell cycle in the late embryonic period in rodent, for instance at E15 in rat retina, and then gradually increase in number (Morrow et al., 1998a,b), in the outer neuroblastic layer (onbl), and later in the outer nuclear layer (ONL). However, expression of Rhodopsin, one of the terminal differentiation markers for rod photoreceptor cells, only begins in the early postnatal period. Previous studies have shown that differentiation of rod photoreceptor cells is to some extent influenced by extrinsic diffusible factors (Altshuler and Cepko, 1992; Altshuler et al., 1993; Kelley et al., 1994; Levine et al., 2000; Lillien, 1995). One of the factors that inhibit rod photoreceptor cell differentiation is reported to be present at a high level in the embryonic retina but downregulated in the postnatal retina, and that factor has been demonstrated to be ciliary neurotrophic factor (CNTF) (Belliveau et al., 2000; Ezzeddine et al., 1997; Kirsch et al., 1998; Levine et al., 2000; Neophytou et al., 1997; Schulz-Key et al., 2002). Since CNTF is present at a high level in the embryonic retina (Kirsch et al., 1997) and downregulated in the early postnatal retina (Kirsch et al., 1997; Schulz-Key et al., 2002), inhibition by CNTF is one of the potential explanations for the lag in rod photoreceptor cell differentiation after cell cycle withdrawal in the embryonic period.

On the other hand, intrinsic regulatory mechanisms (Morrow et al., 1998a; Watanabe and Raff, 1990) involving transcription factors that activate a particular set of terminal marker genes also play important roles in the differentiation of each type of retinal cells. One of the essential transcription factors in activating *rhodopsin* expression is the homeodomain protein, Crx (Chen et al., 1997; Furukawa et al., 1997, 1999, 2002; Livesey et al., 2000). Thus, *crx* should be upregulated to induce rod photoreceptor cell differentiation.

Based on the above, an appropriate combination of extrinsic and intrinsic factors is thought to be necessary for each subset of

* Corresponding author. Department of Physiology, Keio University School of Medicine, Shinanomichi, Shinjuku 160 8582, Tokyo, Japan. Fax: +81-3-3357-5445.
E-mail address: hidokano@sc.itc.keio.ac.jp (H. Okano).
Available online on ScienceDirect (www.sciencedirect.com.)

1044-7431/$ - see front matter © 2004 Elsevier Inc. All rights reserved.
doi:10.1016/j.mcn.2004.02.001

retinal cells to differentiate (Cepko et al., 1996; Edlund and Jessell, 1999; Harris, 1997; Livesey and Cepko, 2001; Watanabe and Raff, 1990). But the underlying mechanisms, especially the interaction between extrinsic and intrinsic factors, still remain to be elucidated. Although CNTF/gp130 is known to function through at least two signaling pathways, that is, the JAK/STAT pathway and the SHP2-RAS/MAPK pathway, no specific mechanism has been assigned to its inhibition of rod photoreceptor cell differentiation.

In this study, we demonstrated that CNTF/gp130 signaling followed by STAT3 activation downregulated both *crx* and Rhodopsin expression. We used conditional knock-out mice devoid of STAT3 activation in the retina and a method of introducing exogenous genes by electroporation that allowed dominant-negative form of STAT3 (STAT3F) to be efficiently expressed in the retinal explants derived from P0 mice (P0 retinal explants), while maintaining the original tissue structure of neural retina. We also demonstrated that STAT3 activation was rapidly downregulated, when presumptive rod photoreceptor cells began to express Rhodopsin and differentiate into rod photoreceptor cells in vivo in the postnatal period. The results showed that persistent activation of STAT3 was responsible for the CNTF-induced inhibition of both *crx* and Rhodopsin expression in the P0 retinal explants. Next, we investigated whether precocious rod photoreceptor cell differentiation occurs before P0 in STAT3-deficient retina. We found neither significant difference in timing of Rhodopsin expression nor upregulation of *crx* expression overall, although we occasionally found a precocious upregulation of *crx* mRNA in STAT3-deficient retinas.

Thus, downregulation of STAT3 activation is required for presumptive rod photoreceptor cells to differentiate in postnatal retina and may contribute as one of the regulatory factors to determine the time of onset of rod photoreceptor cell differentiation. It is likely that several other independent pathways are necessary for proper temporal rod photoreceptor cell differentiation.

Results

Rhodopsin expression in the ONL of P0 retinal explants was inhibited by CNTF

First, we analyzed the effect of CNTF on Rhodopsin expression in P0 retinal explants, in which retinal cells followed developmental processes closely resembling those in vivo (Tomita et al., 1996) (Figs. 1Aa, b, m). Consistent with previous reports (Belliveau et al., 2000; Ezzeddine et al., 1997; Kirsch et al., 1998; Neophytou et al., 1997; Schulz-Key et al., 2002), strong inhibition of Rhodopsin expression in the ONL of P0 retinal explants was observed in the presence of CNTF (50–100 ng/ml) both at day 5 (Fig. 1Ac) and day 10 (data not shown).

The inhibition of Rhodopsin expression by CNTF was not definitive, and the retinal cells resumed expressing Rhodopsin when the CNTF was removed. Rhodopsin-expressing cells appeared in 2 days after removing CNTF following 3–5 days of exposure (Fig. 1Ad), and their expression increased to be observed in most of the cells in the ONL until the end (Fig. 1An). Moreover, the retinal cells in the ONL did not express any markers specific for other cell types examined, that is, HPC-1, PKC-α, and glutamine synthetase (markers for amacrine cells, bipolar cells, and Müller cells, respectively) after CNTF exposure (data not shown). These observations suggested that most presumptive rod photoreceptor cells remained undifferentiated rather than proceeding toward alternative cell fates. Although the possibility that the cells pursuing alternative cell fate in response to CNTF may have migrated from the ONL to other cell layers could not be completely ruled out, the number of such cells, if any, must have been small.

crx transcription in P0 retinal explants was also inhibited by CNTF

To clarify the inhibitory effect of CNTF on the processes leading to Rhodopsin expression, we examined expression pattern of *crx*, which is one of the key transcriptional activators of rod photoreceptor-specific genes including *rhodopsin* (Chen et al., 1997; Furukawa et al., 1997, 1999). *crx* expression is first observed in the outermost layer of the neural retina at E12.5 and spreads over entire ONL and outer half of the inner nuclear layer (INL) in the early postnatal period, eventually becoming restricted to the ONL in adult (Furukawa et al., 1997). The pattern of *crx* expression in retinal explants resembled the pattern in the retina in vivo (data not shown). In control P0 retinal explants at day 5, *crx* expression was observed throughout the entire ONL and outer half of the INL (Fig. 1Ao). After CNTF exposure, however, *crx* expression decreased dramatically in an in situ hybridization experiment performed in parallel (Fig. 1Ap), indicating that downregulation of *crx* expression might contribute to the inhibition of Rhodopsin expression. We further confirmed the downregulation of *crx* expression induced by addition of CNTF using semiquantitative analysis by real-time RT-PCR. After exposure to CNTF for 5 days, the relative level of *crx* mRNA expression in the P0 retinal explants was statistically downregulated to 38.6% (1.0 ± 0.043:0.386 ± 0.032, $P < 0.01$) (Fig. 1B).

STAT3 activation induced by CNTF was closely associated with inhibition of Rhodopsin expression in the ONL cells of P0 retinal explants

To elucidate the molecular mechanism underlying the CNTF-induced inhibition of Rhodopsin expression, we attempted to determine which of the downstream pathways of CNTF/gp130 signaling, the STAT3-mediated pathway or the SHP2-mediated pathway, was responsible for the downregulation of Rhodopsin expression. Following activation of the CNTF/gp130 receptor, STAT3 associates with several tyrosine residues in the gp130 receptor is phosphorylated and forms dimmers, then translocate to the nucleus where it activate the transcription of target genes (Akira, 1999; Takeda and Akira, 2000), whereas SHP2 (protein tyrosine phosphatase 2) associates with another tyrosine residue in the gp130 receptor and activates the RAS/MAPK pathway and/or the PI3 kinase pathway (Hirano et al., 1997; Ohtani et al., 2000).

First, we investigated STAT3 activation by immunohistochemical staining with anti-phosphoSTAT3 antibody. After 5 days of CNTF exposure, phosphorylated STAT3 staining was significantly observed in the nuclei of most ONL cells demonstrating that STAT3 signaling was indeed activated (Fig. 1Ag), but no such staining was seen in onbl cells at day 0 (Fig. 1Ae) nor in control ONL cells (Fig. 1Af). STAT3 activation in the ONL was then quantitatively investigated by immunoblot analysis (Fig. 1C). ONL cell lysates prepared from P0 retinal explants cultured for 5 days with or without exogeneous CNTF were analyzed with anti-STAT3 antibody that recognizes total STAT3 protein including both phosphorylated and unphosphorylated STAT3 proteins, and anti-phosphoSTAT3 antibody that recognizes only phosphorylated STAT3 protein. The amount of total STAT3 protein and phosphorylated STAT3 protein increased 2-fold and 20-fold, respectively, after CNTF exposure. Thus, CNTF induced a 10-fold excess of phosphorylated endogenous STAT3 in ONL cells. We also confirmed the presence of CNTF receptor α in the ONL by immunoblot analysis (data not shown), which was in agreement with the previous reports (Kirsch et al., 1997; Schulz-Key et al., 2002).

Next, double immunostaining revealed a negative correlation between Rhodopsin and phosphorylated STAT3 expression (Figs. 1Ai–l). The cells of P0 retinal explants that failed to express Rhodopsin in the presence of CNTF were ONL cells, in which endogenous STAT3 is highly phosphorylated (Fig. 1Ak). Furthermore, a few phosphorylated STAT3 positive cells, found in the onbl of P0 retinal explants at day 0 (Fig. 1Ai) and in the ONL of P0 retinal explants cultured with CNTF only for the first 3 days followed by CNTF removal (Fig. 1Al), were devoid of Rhodopsin expression (Figs. 1Ai, l). Collectively, these findings demonstrated a negative correlation between STAT3 activation and Rhodopsin expression in P0 retinal explants. Under every condition examined, phosphoSTAT3 positive cells were also observed in the inner layer, where Rhodopsin expression does not occur, in consistent with the previous reports of CNTF receptor expression in retina (Kirsch et al., 1997; Schulz-Key et al., 2002).

STAT3 activation and Rhodopsin expression were negatively correlated in vivo

To determine that STAT3 activation and Rhodopsin expression are negatively correlated in the presumptive rod photoreceptor cells in vivo, we investigated their expression in the onbl at E18.5 and P0. STAT3 activation was observed in most of the cells in the presumptive rod photoreceptor cell layer, the onbl, at E18.5 (Fig. 2Ac), where no Rhodopsin expression was detected (Fig. 2Aa). On the contrary, STAT3 activation was barely seen in the onbl at P0 (Fig. 2Ad), the point in time when Rhodopsin-expressing cells first appeared (Fig. 2Ab). Phosphorylated STAT3 diminished markedly after birth, when Rhodopsin had just begun to be expressed in this layer. A low level of phosphorylated STAT3 remained in cells in the onbl at P0 that did not express rhodopsin (Fig. 2Ah, arrow). In both stages, abundant STAT3 activation was observed continuously in the inner layer (data not shown); however, these cells were unrelated to rhodopsin expression. The STAT3 activation in the onbl was downregulated earlier in the central retina than in the peripheral retina. Correspondingly, Rhodopsin expression started earlier in the central retina than in the peripheral retina. Thus, negative correlation between Rhodopsin expression and STAT3 activation was consistently observed during development of rod photoreceptor cells (Figs. 2Ag, h, high magnification and arrows). Immunoblot analysis further confirmed that the amount of total STAT3 protein and phosphorylated STAT3 protein in the onbl cells at E18.5 were 1.3-fold and 4.5-fold higher, respectively, than at P0 (Fig. 2B).

STAT3 activation, but not SHP2-mediated signaling, was required for CNTF to exert its inhibitory effect on Rhodopsin expression

Based on the above analysis, we hypothesized that the CNTF-induced inhibition of Rhodopsin expression was caused via STAT3 activation. To test this hypothesis, we investigated Rhodopsin expression in P0 retinal explants derived from STAT3 conditional knock-out mice in which STAT3 gene was disrupted only in the retina by using Cre-loxP system. Since STAT3 total knock-out mice could not be used because of embryonic lethality at a very early stage (Takeda et al., 1997), Cre-recombinase expression was directed under control of a retina-specific regulatory element of murine Pax6 (α-Cre) (Marquardt et al., 2001). Cre-recombinase activity was already detectable in E12.5 retina of α-Cre transgenic mice (Baumer et al., 2002; Marquardt et al., 2001). By generating double transgenic mice that carried both the α-Cre and CAG-CAT-GFP transgenes (Kawamoto et al., 2000), we confirmed that α-Cre-mediated recombination indeed occurred in most of the presumptive rod photoreceptor cells, that is, the onbl cells of the P0 retinas except for a few cells possibly due to the variegation of transgene expression (data not shown).

In the absence of exposure to CNTF, P0 retinal explants derived from $STAT3^{flox/-}$;α-Cre mice showed no obvious differences from those derived from their wild-type littermates, at day 0, 5, and 9. However, even after exposure to CNTF for 5 days (100 ng/ml), ONL cells of P0 retinal explants from $STAT3^{flox/-}$;α-Cre mice, in which virtually no phosphorylated STAT3 was detectable (Fig. 3Ac), exhibited Rhodopsin expression at day 5 (Fig. 3Aa); while P0 retinal explants from $STAT3^{flox/+}$ mice, littermates of the mutant mice considered to be phenotypically wild type, did not express Rhodopsin (Fig. 3Ab) with obvious STAT3 activation in the ONL after CNTF exposure (Fig. 3Ad). Furthermore, very small number

Fig. 1. Effects of CNTF on Rhodopsin expression and STAT3 activation in mouse P0 retinal explants. Retinal explants were prepared from P0 neural retina and immediately exposed to 100 ng/ml CNTF at day 0. (A) Double labeling with anti-Rhodopsin antibody and anti-phosphoSTAT3 antibody was performed at day 5, and examined with a confocal microscope. Rhodopsin expression (a–d, m, n). At day 0, a low level of rhodopsin expression was detected in only a few cells in the onbl (a) Control; At day 5, Rhodopsin expression was observed in the ONL (b). At day 5, no Rhodopsin expression was observed after CNTF exposure (c). At day 5, Rhodopsin expression was detected 2 days after CNTF removal following 3 days of exposure to CNTF (d) Control; At day 10, the level of Rhodopsin expression was higher than in "b" (m). Rhodopsin expression had spread throughout the ONL 5 days after CNTF removal following exposure to CNTF for 5 days (n). Detection of phosphorylated STAT3 (e–h). The phosphorylated STAT3 immunoreaction was detected in the nucleus, which was identified by Hoechst staining (data not shown). At day 0, a low level of phosphorylated STAT3 expression was detected in the onbl (e) Control; At day 5, almost no phosphorylated STAT3 expression was observed in the ONL (f). At day 5, a higher level of phosphorylated STAT3 expression was observed in most ONL cells after exposure to CNTF (g). Phosphorylated STAT3 expression was observed in the ONL 2 days after CNTF removal following CNTF exposure for 3 days, but at a lower level than in "g" (h). Merge (i–l). Note that the rhodopsin-expressing cells (arrowheads) in i and l did not express phosphorylated STAT3 and vice versa (arrow). *crx* mRNA expression at day 5 (o, p) Control; A high level of *crx* mRNA was observed in the ONL and outer half of the INL (o). Expression of *crx* mRNA was markedly downregulated after CNTF exposure (p). onbl, outer neuroblastic layer; inbl, inner neuroblastic layer; ONL, outer nuclear layer; INL, inner nuclear layer. (B) Real-time RT-PCR. Relative level of *crx* mRNA expression was statistically downregulated to 38.6% (1.0 ± 0.043:0.386 ± 0.032, $P < 0.01$), after CNTF exposure for 5 days. (C) Immunoblot analysis. Cell extracts were prepared from ONL cells of P0 neural retinal explants cultured with or without CNTF at day 5. After CNTF exposure, the relative amounts of total STAT3 (including both phosphorylated and unphosphorylated STAT3) and phosphorylated STAT3 proteins, measured by NIH image, increased 2-fold and 20-fold, respectively. α-tubulin was used as an inner control.

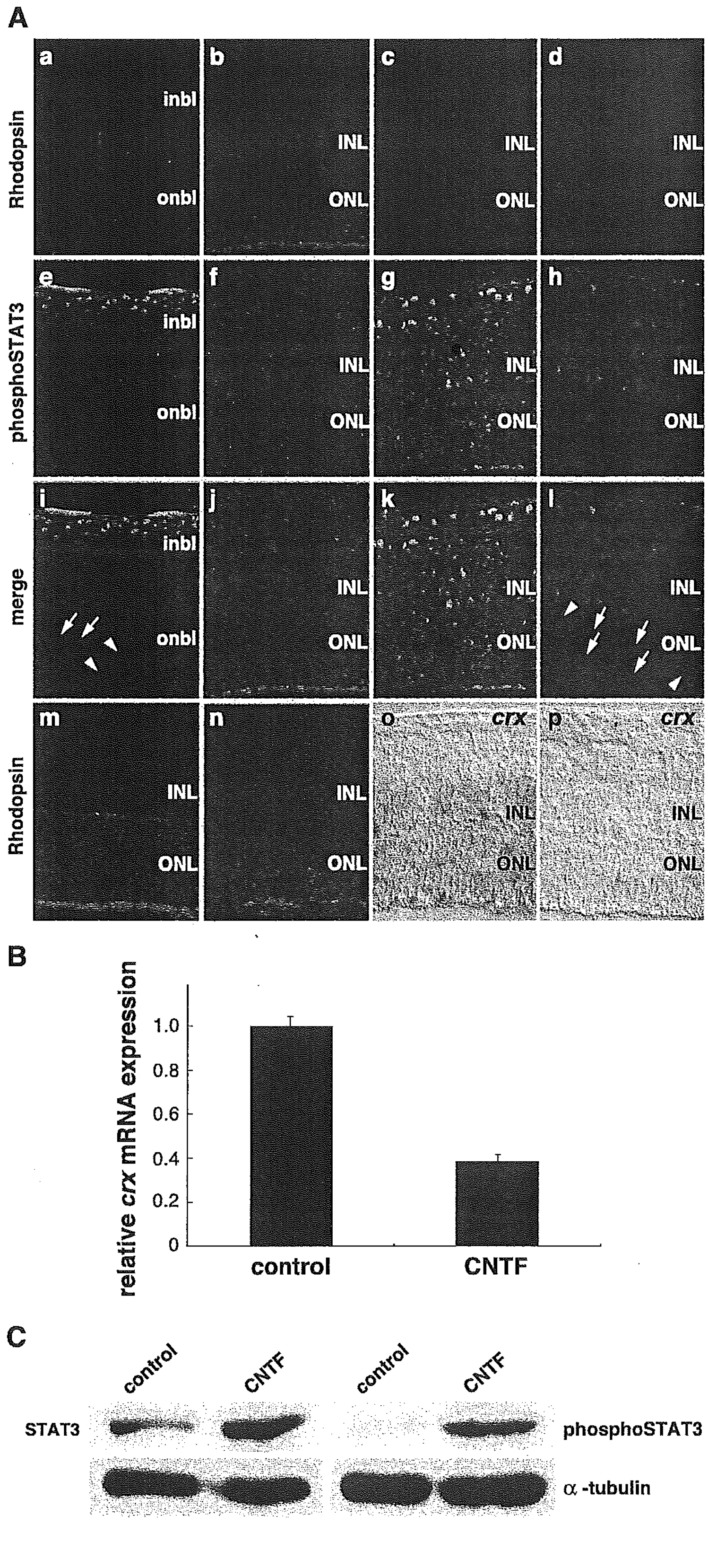
A
a
b
c
d
Rhodopsin
inbl
onbl
INL
ONL
e
f
g
h
phosphoSTAT3
i
j
k
l
merge
m
n
o
p
crx
B
relative crx mRNA expression
1.0
0.8
0.6
0.4
0.2
0
control
CNTF
C
STAT3
phosphoSTAT3
α -tubulin

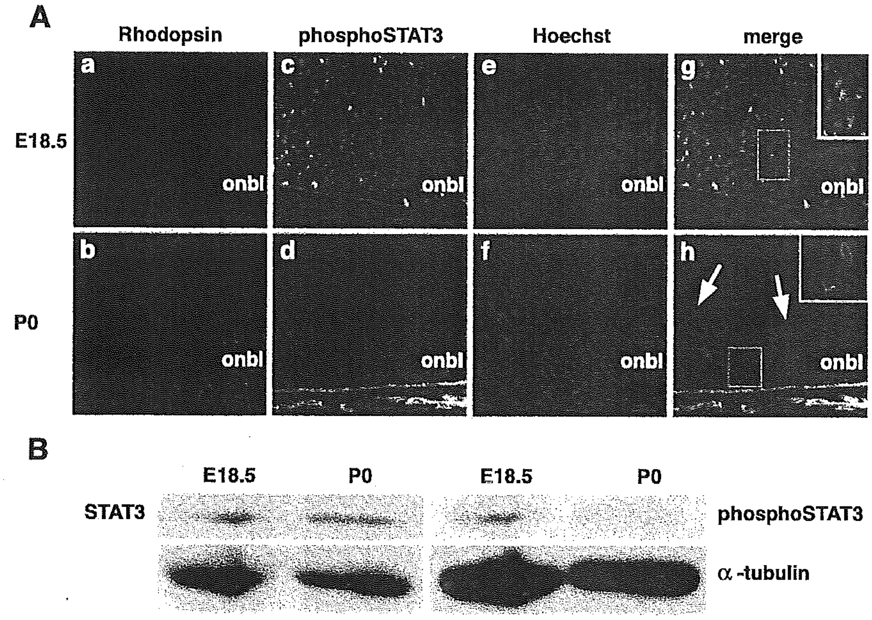

Fig. 2. Rhodopsin expression and STAT3 activation in E18.5 and P0 retina in vivo. (A) At E18.5, no Rhodopsin expression was detected in the onbl (a), whereas a high level of STAT3 activation was observed in the onbl (c). By contrast, at P0, a low level of Rhodopsin expression appeared in the onbl (b), whereas STAT3 activation had diminished markedly in the onbl (d). Phosphorylated STAT3 immunostaining was observed in nuclei (e, f). Merge; STAT3 activation and Rhodopsin expression are negatively correlated (g, h). Insets in g and h: Marked areas are magnified and merged in Hoechst staining images. Rhodopsin was negative in STAT3 activated cells, based on the phosphorylated STAT3 immunoreaction in the nucleus detected by Hoechst staining (inset of g). Rhodopsin-expressing cells showed no STAT3 activation (inset of h). Cells with a low level of phosphorylated STAT3 remaining showed no Rhodopsin expression (h, arrow). onbl, outer neuroblastic layer; inbl, inner neuroblastic layer; ONL, outer nuclear layer; INL, inner nuclear layer; Hoechst staining, blue. (B) Immunoblot analysis. Cell extracts were prepared from onbl cells at E18.5 and P0. Total STAT3 protein and phosphorylated STAT3 protein, measured by NIH image, were 1.3-fold and 4.5-fold higher, respectively, in onbl cells at E18.5 than at P0.

of phosphorylated STAT3 positive cells, which were occasionally found in the ONL probably due to discontinuity of transgene expression as described above, never expressed Rhodopsin with CNTF exposure (Fig. 3Ae). This indicated that only STAT3-deficient cells in the ONL escaped the inhibitory effect of CNTF on Rhodopsin expression.

We also investigated whether STAT3 activation was required for the inhibitory effect of CNTF on *crx* transcription. When cultured in the absence of CNTF, the ONL cells and outer half of the INL cells of P0 retinal explants from both $STAT3^{flox/-}$;α-Cre mice and $STAT3^{flox/+}$ mice expressed comparable levels of *crx* mRNA (Figs. 3Bn, p). Even after CNTF exposure, P0 retinal explants derived from $STAT3^{flox/-}$;α-Cre mice still clearly expressed *crx* mRNA in both the ONL and outer half of the INL (Fig. 3Bm), although at slightly lower level than P0 retinal explants derived from $STAT3^{flox/-}$;α-Cre mice cultured without CNTF. By contrast, retinal cells from $STAT3^{flox/+}$ mice expressed much less *crx* mRNA after CNTF exposure (Fig. 3Bo). This in situ hybridization experiment was performed in parallel. NIH image showed that the relative levels of *crx* mRNA expression after CNTF exposure to the levels of each control were 50% and 15% in $STAT3^{flox/-}$;α-Cre retina and $STAT3^{flox/+}$ retina, respectively. It is true, however, that *crx* mRNA was slightly downregulated by CNTF even in P0 retinal explants from STAT3 conditional knock-out mice, as compared with P0 retinal explants cultured without CNTF. It is possible that an indirect effect of earlier STAT3 gene disruption, for example, STAT family genes, other than STAT3 might have compensated for the loss of STAT3 function and reduced the mRNA level of *crx* instead of STAT3. These results indicated that the differences in expression of *crx* and Rhodopsin were attributable to the difference in STAT3 activation. After CNTF exposure, high level of *crx* expression and Rhodopsin expression were observed only in the absence of STAT3 activation.

To pursue the possibility that the other main pathway of CNTF/gp130 signaling, SHP2-mediated signal, might contribute to the inhibitory effect of CNTF on expression of *crx* and Rhodopsin, we prepared P0 retinal explants from $gp130^{F759}$ knock-in mice homozygotes, in which SHP2 activation was specifically blocked by the Tyr-759 mutation in the gp130 receptor without interfering with STAT3 activation (Ohtani et al., 2000). P0 retinal explants were cultured with CNTF (100 ng/ml) for 5 days. The same as their wild-type littermates, they never expressed Rhodopsin and expressed STAT3 activation obviously in ONL (Figs. 3Ag–l) as predicted. P0 retinal explants derived from $gp130^{F759/F759}$ knock-in mice, as well as those derived from their wild-type littermates, expressed a high level of *crx* in the absence of CNTF (Figs. 3Br, t), and exhibited markedly downregulated *crx* expression when exposed to CNTF (Figs. 3Bq, s). Semiquantification by NIH image showed that CNTF exposure induced downregulation of *crx* mRNA in $gp130^{F759/F759}$ knock-in retina as well as in wild-type retina (the relative levels of *crx* mRNA expression after CNTF exposure to the levels of each control were 5% and 13% in $gp130^{F759/F759}$ knock-in retina and wild-type retina, respectively). Thus, these findings indicated that SHP2 activation is not responsible for the effect of CNTF on Rhodopsin expression.